

A population framework for predicting the proportion of people infected by the far-field airborne transmission of SARS-CoV-2 indoors

Christopher Iddon^a, Benjamin Jones^{a,*}, Patrick Sharpe^a, Muge Cevik^b,
Shaun Fitzgerald^c

^a*Department of Architecture and Built Environment, University of Nottingham,
Nottingham, UK*

^b*Department of Infection and Global Health, School of Medicine, University of St
Andrews, St Andrews, UK*

^c*Department of Engineering, Cambridge University, Cambridge, UK*

Abstract

The number of occupants in a space influences the risk of far-field airborne transmission of SARS-CoV-2 because the likelihood of having infectious and susceptible people both correlate with the number of occupants. This paper explores the relationship between occupancy and the probability of infection, and how this affects an individual person and a population of people. Mass-balance and dose-response models determine far-field transmission risks for an individual person and a population of people after sub-dividing a large *reference* space into 10 identical *comparator* spaces.

For a single infected person, the dose received by an individual person in the *comparator* space is 10-times higher because the equivalent ventilation rate per infected person is lower when the *per capita* ventilation rate is preserved.

*Corresponding author

Email address: benjamin.jones@nottingham.ac.uk (Benjamin Jones)

Preprint submitted to Indoor Air

February 3, 2022

However, accounting for population dispersion, such as the community prevalence of the virus, the probability of an infected person being present and uncertainty in their viral load, shows the transmission probability increases with occupancy and the *reference* space has a higher transmission risk. Also, far-field transmission is likely to be a rare event that requires a high emission rate, and there are a set of Goldilocks conditions that are *just right* when ventilation is effective at mitigating against transmission. These conditions depend on the viral load, because when they are very high or low, ventilation has little effect on transmission risk.

Nevertheless, resilient buildings should deliver the equivalent ventilation rate required by standards as minimum.

Keywords: relative exposure index, ventilation, aerosols, transmission risk, viral load, COVID-19

1 Nomenclature

2 \bar{I} mean number of infected people in a space that contains a potential
3 transmission event

4 $\overline{P(R)_I}$ mean individual probability of infection occurring in each space

5 $\overline{P(R)}$ mean individual infection risk that occurs in all spaces with a potential
6 transmission

7 ϕ total removal rate (s^{-1})

8 C community infection rate

9 D dose (viable virions)

10 G emission rate of RNA copies (RNA copies s^{-1})

11 I number of infected people

12 K fraction of aerosol particles absorbed by respiratory tract

13 k reciprocal of the probability that a single pathogen initiates an infec-
14 tion

15 L viral load (RNA copies ml^{-1} of respiratory fluid)

16 N number of occupants

17 N_s number of susceptible people exposed

18 $N_s(I)$ number of susceptible people exposed in spaces that contain I infected
19 people

- 20 N_t number of transmissions for an entire population
- 21 $N_t(I)$ number of transmissions that occur in spaces that contain I infected
22 people
- 23 N_{pop} population size
- 24 $P(0 < I < N)$ probability of a space containing a potential transmission
- 25 $P(I)$ probability of I infected people present
- 26 $P(L)$ probability of a viral load
- 27 $P(R)$ individual infection probability for a given dose
- 28 $P(S)$ probability of a person being both susceptible and exposed to the virus
- 29 PPI proportion of a population infected
- 30 q_{resp} respiratory rate ($\text{m}^3 \text{s}^{-1}$)
- 31 T exposure period (s)
- 32 TR transmission ratio
- 33 V space volume (m^3)
- 34 v viable fraction of RNA copies

35 **1. Introduction**

36 Severe Acute Respiratory Syndrome Coronavirus 2 (SARS-CoV-2) is a
37 virus that causes COVID-19. In 2020, it spread rapidly worldwide causing

38 a pandemic. The primary mode transmission of the virus occurs when it is
39 encapsulated within respiratory droplets and aerosols and inhaled by a sus-
40 ceptible person [1]. These are most concentrated in the exhaled puff of an
41 infected person, which includes a continuum of aerosols and droplets of all
42 sizes as a multiphase turbulent gas cloud [2, 3]. The subsequent transport
43 of infectious aerosols from the exhaled puff occurs differently in outdoor and
44 indoor environments. Outside, air movement disrupts the exhaled puff, a
45 prodigious space volume rapidly dilutes it [4], and ultra-violet (UV) light
46 renders the virus biologically non-viable over a short period of time [5]. In-
47 side, the magnitude of air movement is usually insufficient to disrupt the
48 exhaled puff, a finite space volume and lower ventilation rates concentrate
49 aerosols in the air, and there is usually less UV light [6]. Accordingly, trans-
50 mission of the virus occurs indoors more frequently than outdoors [7, 8], and
51 inhaling the exhaled puff at close contact is more likely to lead to an infec-
52 tive dose than when inhaling indoor air at a distance where the virion laden
53 aerosols are diluted. This is consistent with the epidemiological understand-
54 ing that SARS-CoV-2 is spread primarily by close contact where it might be
55 possible to smell a person’s *coffee breath* [2, 3, 9, 10, 11]. However, it is still
56 possible for a susceptible person to inhale an infective dose of aerosol borne
57 virus, from shared indoor air, known as *far-field* airborne transmission, and
58 occurs at distances of > 2 m from the infected person. Far-field transmis-
59 sion is linked to several super spreading events and is often correlated with
60 poor indoor ventilation, long exposure times, and respiratory activities that
61 increase aerosol and viral emission, such as singing [12, 13, 14].

62 Previous analyses of far-field infection risk consider the presence of a single

63 infected person. However, the number of occupants in a space influences the
64 risk of airborne transmission because the likelihood of having infectious and
65 susceptible people both scale with the number of occupants. Therefore, it
66 may be advantageous to sub-divide large spaces into a number of identical
67 smaller spaces to reduce the transmission risk. Here, the space volume and
68 ventilation rate per person would be kept constant, and occupants equally
69 divided into smaller groups of people. The impact of this strategy on virus
70 transmission is not obvious. On one hand, the smaller space with lower
71 occupancy reduces the probability of an infected person being present, and
72 also reduces the number of susceptible people who are exposed to infected
73 people. On the other hand, the ventilation rate per infected person is likely
74 to be smaller in the smaller space, increasing the transmission risk for any
75 susceptible people present. Accordingly, this paper explores the relationship
76 between occupancy and the probability of infection, and how this affects an
77 individual person and a population of people. We take a theoretical approach
78 to consider the infection risk for the population of a large space and compare
79 it to the same population distributed in a number of smaller identical spaces.

80 We first consider the infection risk for a person using an existing analytical
81 model [15] to predict the dose, and the probability that the dose leads to
82 infection, in a big and a small space. We then consider the infection risk for
83 two equal populations distributed evenly in either the big space or a number
84 of smaller spaces, by considering the community infection rate, the viral load,
85 and the probability of infection from a viral dose.

86 Section 2 outlines the modelling approach and the input data. Section 3
87 considers the personal risks from sub-division and Section 4 considers the

88 risks for a population. Section 5 discusses factors that affect infection risk
89 and limitation of the work.

90 2. Theoretical approach

91 An analytical model is used to predict the dose of viral genome copies of
92 an individual person and associated individual and population infection risks
93 of infection.

94 2.1. Dose and infection risk

95 The mass-balance model of Jones *et al.* [15] is used to predict the num-
96 ber of RNA copies absorbed by the respiratory tract of a person exposed to
97 aerosols in well mixed air over a period of time that is sufficient for the vi-
98 able virus concentration to reach a steady-state, and then combined with the
99 viable fraction, v , to give a dose, D .

$$D \simeq \frac{K q_{resp} G T v}{\phi V} \quad (1)$$

100 Here, K is the fraction of aerosol particles absorbed by respiratory tract,
101 q_{resp} is the respiratory rate ($\text{m}^3 \text{s}^{-1}$), G is the emission rate of RNA copies
102 (RNA copies s^{-1}) and is a function of the respiratory activity (see Jones *et*
103 *al.*), T is the exposure period (s), ϕ is the total removal rate (s^{-1}), which
104 represents the sum of all removal by ventilation, surface deposition, biological
105 decay, respiratory tract absorption, and filtration, and V is the space volume
106 (m^3). The product ϕV can be considered to be an *equivalent* ventilation
107 rate. The approach is common and has been used by others to investigate
108 exposure in well mixed air [16, 17].

109 For a full description of the model, a discussion of uncertainty in suitable
110 inputs, and a sensitivity analysis, see Jones *et al.* [15]. The analysis shows
111 that the most sensitive parameter is G , the rate of emission of RNA copies.
112 G is a function of the *viral load* in the respiratory fluid, L (RNA copies ml⁻¹)
113 and the volume of aerosols emitted, which in turn is a function of exhaled
114 breath rate and respiratory activity; see Appendix A. The distribution of
115 the viral load within the infected population is reported to be log-normal by
116 Yang *et al.* [4], Weibull by Chen *et al.* [18], and Gamma by Ke *et al.* [19].
117 This suggests that the true distribution is unknown and so we use the data
118 of Chen *et al.* [20] who predict that log₁₀ values of viral load are normally
119 distributed with a mean of 7 log₁₀ RNA copies ml⁻¹; see Table 2 and Figure 2.
120 We explore variations in these values in Section 2.3 and discuss their origin,
121 and uncertainty in them, in Section 5.5. The probability of a viral load,
122 $P(L)$, can then be determined from a Gaussian probability density function.

123 The dose can be used to estimate a probability of infection using a dose-
124 response curve. However, there is no dose-response curve for SARS-CoV-2.
125 A number of studies [21, 16, 22] apply a dose curve for the SARS-CoV-1 virus,
126 which is a typical dose curve for corona viruses, and so it is applied here.
127 There are obvious problems with this extrapolation and they are discussed
128 in Section 5.5. The probability of infection of an individual person, $P(R)$, is
129 assumed to follow a Poisson distribution

$$P(R) = 1 - e^{-D/k} \quad (2)$$

130 where, k is the reciprocal of the probability that a single pathogen initiates
131 an infection. When $D = k$, $P(R) = 63\%$. We use a value of $k = 410$ following

132 DeDiego *et al.*[23].

133 2.2. Individual risk

134 A Relative Exposure Index (REI) is used to compare exposure risk for
135 an individual person between two spaces following Jones *et al.* [15]. This
136 approach has already been used to inform national policy on the role of
137 ventilation in controlling SARS-CoV-2 transmission and to identify the ap-
138 propriate application of air cleaning devices [24, 25].

139 The REI is the ratio of the dose, D , received by a susceptible occu-
140 pant in each of two spaces using Equation 1 where the *reference* space is
141 the denominator and the *comparator* space is the numerator. An advan-
142 tage of using an REI is that uncertainty in the viral load of respiratory
143 fluid (RNA copies ml⁻¹), which is used to determine the viral emission rate,
144 G (RNA copies m⁻³), and the unknown dose response both cancel allowing
145 scenarios to be compared. When the REI is > 1 the comparator space is
146 predicted to pose a greater risk to an individual susceptible occupant be-
147 cause they inhale a larger dose, although the absolute risk that this dose will
148 lead to a probability of infection is not considered. Any space that wishes to
149 have a REI of unity or less, must at least balance the parameters in Equa-
150 tion 1. A limitation of the REI is that it does not consider the probability
151 of encountering an infected person with the same viral load in each scenario.

152 2.3. Population infection risk

153 The probability that a number of infected people, I , is present in a space,
154 $P(I)$, as a function of the number of occupants, N , is determined by con-
155 sidering the community infection rate, C , and standard number theory for

156 combinations.

$$P(I) = \frac{C^I(1-C)^{(N-I)}N!}{I!(N-I)!} \quad (3)$$

157 When a large population of people, N_{pop} , is divided into a number of identical
158 spaces, the total number of transmissions, N_t , that occur is the sum of the
159 number of transmissions that occur in each space.

$$N_t = \sum_{I=1}^{N-1} N_t(I) \quad (4)$$

160 where $N_t(I)$ is the number of transmissions that occur in spaces that contain
161 I infected people. For a large population, the number of people infected in
162 each space is the product of the number of susceptible people exposed, N_s ,
163 and the mean individual probability of infection in each space, $\overline{P(R)}_I$.

$$N_t = \sum_{I=1}^{N-1} N_s(I)\overline{P(R)}_I \quad (5)$$

$$N_s(I) = P(I)N_{pop}N^{-1}(N-I) \quad (6)$$

164 where $N_s(I)$ denotes the number of susceptible people exposed in spaces
165 that contain I infected people, $P(I)$ is the probability that a space contains
166 I infected people, and $N_{pop}N^{-1}$ denotes the total number of spaces that
167 occur when a population N_{pop} is divided into groups of N people. Here, the

168 proportion of the population newly infected is given by

$$PPI = \frac{N_t}{N_{pop}} = \sum_{I=1}^{N-1} P(I) \frac{N-I}{N} \overline{P(R)_I} \quad (7)$$

169 The exact solution for Equation 7 becomes increasingly difficult to eval-
170 uate as the space size increases. The calculation complexity is unlikely to
171 be justified given the uncertainties in both the modelling assumptions and
172 the available data. Therefore, simple approximations to the equation are
173 desirable.

174 One approach is to express the number of transmission events using a
175 single mean individual risk for all possible transmissions. Here, the PPI can
176 be expressed as

$$PPI = P(S) \overline{P(R)} \quad (8)$$

177 where $P(S)$ is the proportion of the population who are both exposed and
178 susceptible, and $\overline{P(R)}$ is the average individual infection risk that occurs in
179 all spaces where there is a potential transmissions.

180 Transmission events can only occur when there are both one or more
181 infected people present in a space ($I > 0$) and one or more susceptible people
182 are present ($I < N$). It follows that the probability of a space containing a
183 potential transmission event is given by

$$P(0 < I < N) = 1 - C^N - (1 - C)^N \quad (9)$$

184 As the number of occupants tends to infinity, the probability that the space
185 contains a potential transmission event approaches one, and is equal to zero

186 for single occupancy spaces. This suggests that it may be better to partition
187 a large space; see Section 1. Each space contains $(N - I)$ susceptible people
188 and the probability that an occupant is both susceptible and exposed is the
189 difference between the number of susceptible people in the wider population,
190 $(1 - C) N_{pop}$, and the number of susceptible people who are not exposed,
191 $P(0) N_{pop}$. Therefore, $P(S)$ is given by

$$P(S) = (1 - C) - (1 - C)^N \quad (10)$$

192 This equation shows that $P(S)$ approaches the proportion of susceptible peo-
193 ple in the wider population as $N \rightarrow \infty$. $P(S)$ can be minimised by reducing
194 the community infection rate.

195 Evaluating the mean individual risk is non-trivial. Here an approximation
196 is used, where

$$\overline{P(R)} = \int_1^\infty P(L) \left(1 - e^{-\frac{D}{k} \bar{I}}\right) dL \quad (11)$$

197 Here, $P(L)$ is the probability of an infected person having a viral load L ,
198 and \bar{I} denotes the mean number of infected people in a space that contains
199 a potential transmission event, and is given by

$$\bar{I} = \frac{N (C - C^N)}{P(0 < I < N)} \quad (12)$$

200 This allows the proportion of people infected in a scenario to be approximated

201 by

$$PPI \approx P(S) \int_1^{\infty} P(L) \left(1 - e^{-\frac{D}{k} \bar{I}}\right) dL \quad (13)$$

202 A transmission ratio, TR , gives an indication of the relative risk of infec-
203 tion between a *reference* and a *comparator* space where

$$TR = PPI_{comparator} / PPI_{reference} \quad (14)$$

204 2.4. Scenarios

205 The probabilities given in Section 2.3 can be used to consider how the
206 number of occupants may affect the relative exposure risk at population scale.
207 First, we define a reference space against which others are compared. This
208 space is an office, which is chosen because it is common and well regulated
209 in most countries with consistent occupancy densities. The reference space
210 has an occupancy density of 10 m^2 per person, a floor to ceiling height of 3 m,
211 and an outdoor airflow rate of 10 l s^{-1} per person. There are 50 occupants
212 who are assumed to be continuously present for 8 hours breathing for 75% of
213 the time and talking for 25%. Hereon it is known as the Big Office.

214 Then, we define a comparator space by subdividing the 50 person office
215 into 10 identical spaces. Each space preserves the occupancy density, the *per*
216 *capita* space volume, the outdoor airflow rate per person, and the air change
217 rate. Hereon each comparator space is known as the Small Office.

218 All scenario inputs are given in Table 1.

Table 1: General scenario inputs (top) and calculations of individual risk (bottom).

	Big Office Reference	Small Office Comparator
Number of occupants, N	50	5
Space Volume, V (m^3)	1500	150
Air flow rate, ψV (ls^{-1})	500	50
Equivalent ventilation rate, ϕV (ls^{-1})	942	94.2
Air change rate, ψ (h^{-1})		1.2
Removal rate, ϕ (h^{-1})		2.26
<i>Per capita</i> volume, $V N^{-1}$ (m^3 per person)		30
Exposure time, T (h)		8
Dose constant [23], k		410
Respiratory tract absorption fraction, K		0.55
Viable fraction, v (%)		100
Respiratory activity, <i>breathing: talking</i> (%)		72:25
Volumetric ratio of exhaled droplets to exhaled air, V_{drop}^*	5.05×10^{-13}	
Respiratory fluid density (ml m^{-3})	1.25×10^8	
Respiratory rate, q_{resp} ($\text{m}^3 \text{h}^{-1}$)	0.56	
Viral emission rate, G (RNA copies h^{-1})	394	
Community infection rate, C	1:100	
Viral load [20], L (RNA copies ml^{-1})		1×10^7
Dose, D (viable virions inhaled)	0.245	2.450
REI	1	10

All values converted to SI units before application.

219 2.5. Probabilistic estimates

220 A Monte Carlo (MC) model is used to corroborate the theory given in
 221 Section 2.3 and to investigate overdispersion in the model in Section 5.1.
 222 Pseudocode is given in Appendix B and MATLAB code is available under a
 223 creative commons license contained within the Supplementary Materials¹

224 A population of 1×10^7 people is divided into a number of identical

¹ <https://doi.org/10.1101/2021.11.24.21266807v3>

Table 2: Scenario inputs (top) and calculations of population risk (bottom) given to 2 significant figures.

	Big Office Reference	Small Office Comparator
Viral load [20] (\log_{10} RNA copies ml^{-1})	N(7,1.4)	
Population, N_{pop}	1×10^7	
Number of spaces	2×10^6	2×10^5
Probability of transmission event, $P(0 < I < N)$ (%)	39	4.9
Probability of susceptible people, $P(S)$ (%)	38	3.9
Mean number of infected people [‡] , \bar{I}	1.3	1.0
Mean emission rate [†] (RNA copies h^{-1})	2.5×10^4	2.6×10^3
Mean emission rate [‡] (RNA copies h^{-1})	6.3×10^4	5.4×10^4
Mean dose [†] (virions inhaled)	17	18
Mean dose [‡] (virions inhaled)	44	370
Mean probability of infection [†] (%)	1.3	0.48
Mean probability of infection [‡] , $\overline{P(R)}$ (%)	3.2	9.8
Proportion of population infected, PPI (%)	1.2	0.38
Transmission ratio, TR	1	0.31

N, normal(μ, σ); †, all spaces; ‡, spaces where infected people present.

225 spaces, which varies depending on the scenario; see Section 2.4 and Table 2.
 226 The population size is chosen so that the values of PPI and TR , rounded
 227 to two significant figures, do not change when the MC code is rerun. A
 228 binomial distribution can be used to model the number of successes in a
 229 number of independent trials, and so it is used to model both the number of
 230 infected people in each space and the number of susceptible people who are
 231 then infected when they inhale a dose of the virus. All inputs are given in
 232 Tables 1 and 2.

233 Uncertainty in other inputs are not explored because this has been done
 234 before [15] and to focus this work on an exploration of uncertainty in the
 235 viral load and the community infection rate.

236 3. Individual risk

237 The REI is the ratio of the dose predicted using Equation 1 for Big Office
238 and Small Office; see Section 2.2. When the number of infected people and
239 their respiratory activities, and the breathing rates of susceptible occupants,
240 are identical in each space, the REI simplifies to a ratio of equivalent ven-
241 tilation rates, ϕV . The equivalent ventilation rate is used to determine the
242 steady state concentration of viable virions. Table 1 shows that the removal
243 rate ϕ is identical in both spaces and so the REI becomes a simple ratio
244 of the number of occupants. This suggests that, in the presence of a single
245 infected person, the relative risk is 10 times higher in the Small Office. This
246 occurs because the Small Office contains ten times fewer people than the Big
247 Office, and therefore the ventilation rate *per infector* is ten times smaller.

248 The equivalent ventilation rate per person, $\phi V N^{-1}$, is identical in both
249 spaces and, if it is desirable to preserve the equivalent ventilation per person
250 in two different spaces, the space volume per person must be preserved.

251 The removal rate, ϕ , includes the biological decay of the virus and the
252 deposition of aerosols onto surfaces. Both of these removal mechanisms are
253 space-volume dependent, and so their contribution to the removal of the
254 virus is greater in spaces with a larger volume. Therefore, increasing the
255 space volume per person also has the effect of reducing the REI. This has
256 obvious physical limitations and a simpler approach is to reduce the number
257 of people per unit of volume.

258 Equation 1 is used to calculate the dose of viable virions in each space
259 and Table 1 shows that the magnitudes of the doses are small. There is great
260 uncertainty in these values, attributable to modelling assumptions and in the

261 inputs given in Table 1, but an increase by an order of magnitude still leads
262 to a small dose. This fact is compounded by the value of unity for the viable
263 fraction, which has the effect that all RNA copies inhaled are viable, which
264 is unlikely. A viable fraction of unity was chosen because its true value is
265 currently unknown, and this assumption simplifies the analysis. The value
266 is clearly likely to be $\ll 100\%$ in reality, and so the actual doses would be
267 substantially lower than those estimated here. This suggests that far-field
268 transmission in buildings requires high viral emission rates, G , which are
269 likely to be a rare event.

270 The probability of an infection occurring when a susceptible occupant is
271 exposed to the dose reported in Table 1 is estimated using Equation 2 to
272 be $P(R) < 1\%$ for both spaces and is approximately 10 times greater in the
273 Small Office; see Table 2. Generally, this shows that the viral load has to
274 be greater in the Big Office than in the Small Office to achieve the same
275 $P(R)$ when $C < 1\%$. This is demonstrated by Figure 2, which describes the
276 relationship between the viral load in respiratory fluid (RNA copies ml^{-1}) in
277 each space attributable to any number of infected people and the consequent
278 $P(R)$ for a susceptible occupant, if the virus emission rate, G , is assumed to
279 be linearly related to the viral load, L , of the infected person.

280 For any viral load the dose is calculated using Equation 1, and the prob-
281 ability that it leads to an infection is calculated using Equation 2. This
282 creates a dose-response curve for both scenarios where factors that influence
283 the REI and, therefore, the dose, determine the viral loads necessary to lead
284 to a specific probability of infection. It also shows the relationship between
285 the viral load and the probability that a single infected person has that viral

286 load, $P(L)$. The dotted vertical lines show the viral load required to give
287 a 50% probability that the dose will lead to an infection for each scenario,
288 $P(R) = 50\%$. The area under the viral load probability density curve to the
289 right of each vertical line is the probability that the viral load of the infected
290 person leads to $P(R) \geq 50\%$. The probability is much smaller for the Big
291 Office, which has the lower REI. This probability that an infected person has
292 a viral load that leads to $P(R) \geq 50\%$ is small, suggesting that the most
293 likely outcome is $P(R) \leq 50\%$. There is great uncertainty in the magnitude
294 of these values, particularly in $P(R)$ and in the conversion of a viral load to
295 a virus emission rate (see Section 2), but significant increases in them do not
296 change the general outcomes of the analysis. More generally, increasing the
297 number of occupants in a space while preserving the *per capita* volume has
298 the effect of moving the $P(R)$ curve to the right in Figure 2 and towards the
299 tail of the $P(L)$ curve, which reduces the likelihood that infected people in
300 the space have a sufficient viral load.

301 The $P(L)$ distribution curve could be flattened and shifted to the left of
302 Figure 2 by reducing the viral load of the infected population. For example,
303 vaccination is shown to clear the virus from the body quicker in infected
304 vaccinated people, which at a population scale could flatten the distribution
305 of $P(L)$ [26]. However, different variants of the SARS-CoV-2 virus could
306 increase the viral load, or the proportion of viable virions, or the infectivity
307 of virions, and move the curve to the right of Figure 2 [27, 28]. Other respi-
308 ratory viruses have different distributions of the viral load but the principles
309 described here can be applied to them too.

310 **4. Population risks**

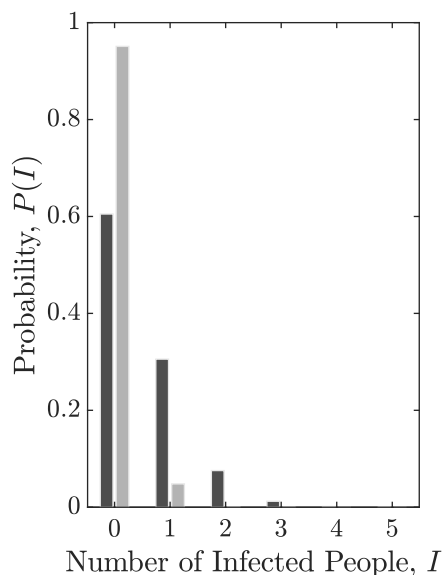


Figure 1: The probability of a number of infected people, I , present in the Big Office (dark) and Small Office (light), $P(I)$, when $C = 1\%$.

311 The analysis in Section 3 is underpinned by the assumption that there is a
312 single infected person in each space. When the community infection rate (C)
313 is known, Equation 3 can be used to estimate the probability that a specific
314 number of infected people are present. Figure 1 shows that when $C = 1\%$,
315 in the Big Office $P(I = 0) = 61\%$, $P(I = 1) = 31\%$, and $P(I > 1) = 9\%$.
316 For the Small Office, $P(I = 0) = 95\%$, $P(I = 1) = 5\%$, and $P(I > 1)$ is
317 negligible. This shows that the Big Office is 8 times more likely to have an
318 infected person present than the Small Office, although Table 1 shows that
319 the relative risk is 10 times smaller in the Big Office than the Small Office
320 when a single infected person is present. However, it is much more likely
321 that both spaces do not have an infected person present, but when they are,

322 the most likely number of infected people is 1. Equation 12 shows that the
323 mean number of transmissions is $\bar{I} \geq 1$ for both scenarios when $C = 1\%$.

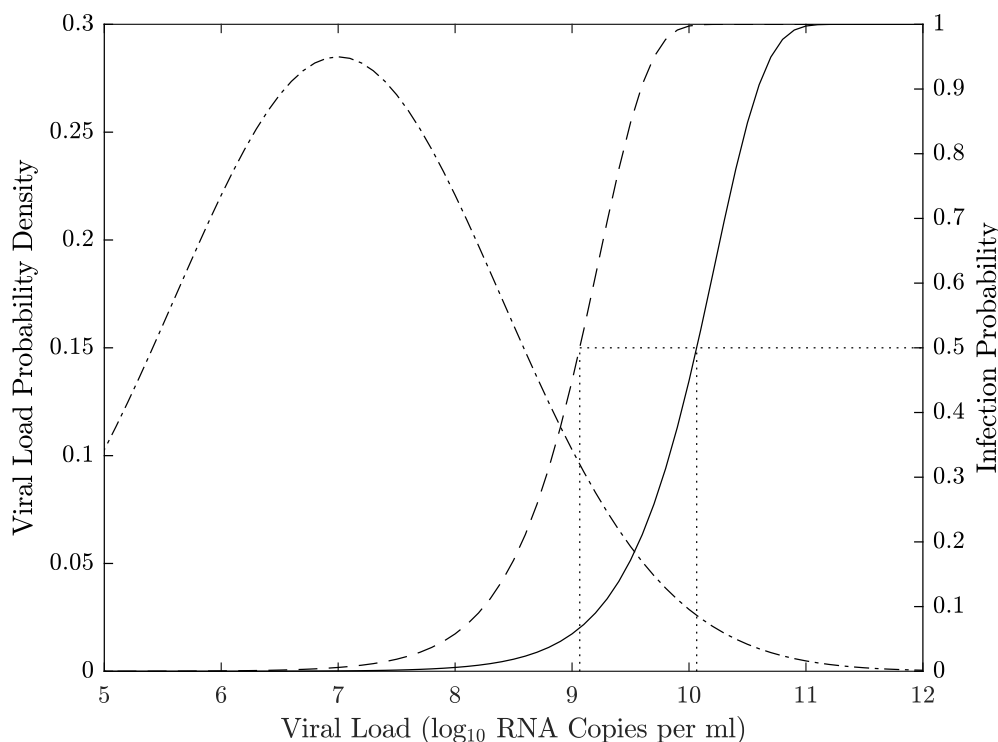


Figure 2: An indication of the relationship between the viral load, L , and the consequent probability of infection, $P(R)$, in the Big Office (solid) and Small Office (dash) for a susceptible occupant, and the probability of a single infected person having a viral load, $P(L)$, (dot-dash). Dotted vertical lines indicate the viral load required for $P(R) = 50\%$.

324 Figure 2 shows the relationship between the probability of infection and
325 the probability of a person having a particular viral load. The viral load that
326 leads to an infection can be attributed to any number of infected people, but
327 the probability of having more than 1 infected person in a space is generally
328 small unless $N > C^{-1}$; see Equation 9. When only 1 infected person is
329 assumed to be present, Figure 2 also shows that the most probable viral
330 loads are highly unlikely to lead to an infection in either the Small Office

331 or the Big Office. Therefore, the infected person must have a significant
332 viral load to infect susceptible occupants, which is an improbable event. The
333 infection risk for susceptible occupants is lower in the Big Office than the
334 Small Office when only 1 infected person is present.

335 Bigger spaces that preserve the *per capita* volume given in Table 1, and
336 where $N \gg 50$, have a higher probability of susceptible people, $P(S)$, and
337 infected people, $P(0 < I < N)$. The effect on the aerosol concentration and
338 the dose depends on the space volume per infected person, $V I^{-1}$, relative
339 to that of the Reference Space, the Big Office. If $V I^{-1}$ decreases, then the
340 aerosol concentration, the dose, and the probability of infection, $P(R)$, all
341 increase. Accordingly, spaces with a high volume per occupant have a lower
342 infection risk. Here, spaces with high ceilings or low occupancy densities are
343 advantageous.

344 An increase in C also increases the probabilities of the presence of in-
345 fected people, $P(0 < I < N)$, and susceptible people, $P(S)$, in any space.
346 This increases the total viral load, the dose, D , and the probability of in-
347 fection, $P(R)$. Accordingly, maintaining a low community infection rate is
348 important. It is worth noting that C may vary by region, or by a particular
349 population demographic [29, 30]. Then, it is appropriate to use C for that
350 demographic, rather than using a national value. It is possible to assess C by
351 taking randomised samples from the population, such as the UK Coronavirus
352 (COVID-19) Infection Survey [31], which includes all infected people at all
353 stages of the disease. However, this survey includes symptomatic people who
354 are likely to be isolating and so the actual C is likely to be lower.

355 The information in Figure 2 can be combined to determine the total

356 proportion of people newly infected, PPI , in a space for all viral loads as a
357 function of the probability that an individual infected person has a particular
358 viral load, $P(L)$, the probability of the risk of infection, $P(R)$, the probability
359 of the presence of susceptible people $P(S)$, and the average number of infected
360 people, \bar{I} ; see Equations 7 and 8.

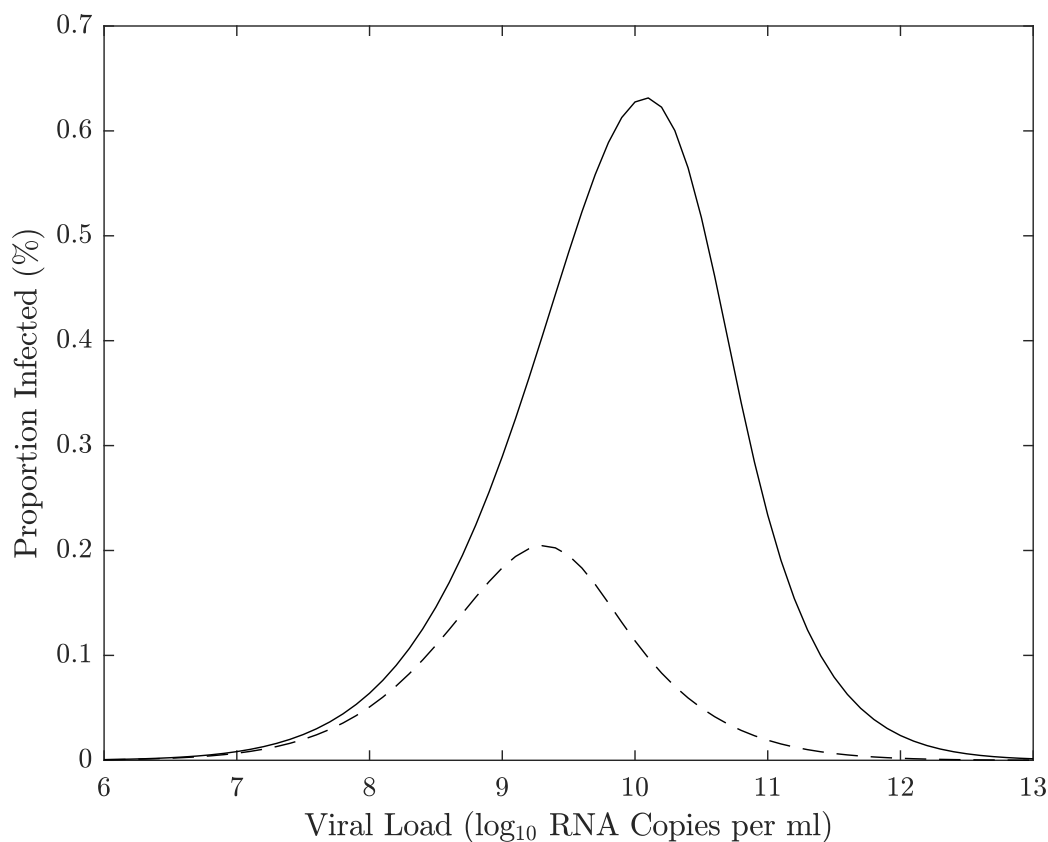


Figure 3: An indication of the relationship between the proportion of a population infected for a particular viral load when the community infection rate is $C = 1\%$. The area under the curve represents the total proportion of people infected for the Small Office (dash) and the Big Office (solid).

361 Figure 3 shows the relationship between the PPI and the viral load where
362 the area under each curve is the proportion of the entire population infected

363 when $C = 1\%$ and assuming that two equal populations are each distributed
364 evenly across a number of spaces; the first across a number of Big Office
365 spaces and the second distributed across a larger number of Big Office spaces.
366 The area under the curve and thus the values for the population PPI are
367 confirmed using the MC analysis described in Section 2.5 and given in Table 2.
368 Table 2 indicates that the probability of far-field infection is $PPI = 0.38\%$
369 in the Small Office and $PPI = 1.2\%$ in the Big Office. The TR is calculated
370 using Equation 14 and is 0.31. Therefore, the infection risk is 3 to 4 times
371 higher in the Big Office.

372 The absolute values of PPI are likely to be much smaller than those
373 calculated here because of the conservative assumptions used to estimate
374 the viral emission from the viral load (see Section 2.1), so the PPI may
375 well be $\ll 1\%$ in both spaces using less conservative assumptions; see the
376 Supplementary Materials¹. This indicates that although there are benefits of
377 subdividing for a population, their magnitude needs to be considered against
378 other factors, such as the overall work environment, labour and material
379 costs, and inadvertent changes to the ventilation system and strategy.

380 The uncertainties in all of the values given here are significant and so
381 it is not possible to be confident in the magnitude of the PPI or the TR ,
382 but testing the model with a range of assumptions enables an assessment of
383 general trends; for example, how increasing occupancy and preserving *per*
384 *capita* space volume and ventilation rates impact the risk of infection and
385 how different mitigation measures, such as increasing the ventilation rate,
386 affect the relative PPI . These are discussed in Section 5.

387 **5. Discussion**

388 *5.1. Overdispersion*

389 The MC approach described in Section 2.5 was used to corroborate the
390 mathematics given in Section 2.3. The predictions given in Table 2 can
391 be produced using either method, giving confidence in the concept and the
392 model.

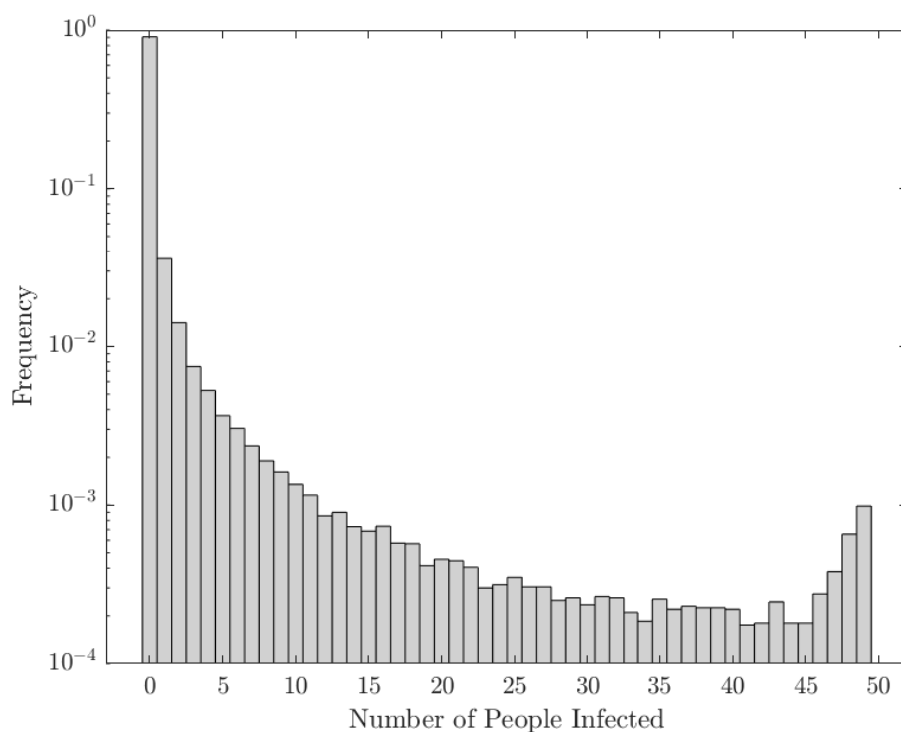


Figure 4: The number of susceptible people infected in each Big Office space estimated using a Monte Carlo approach.

393 The MC approach is used to interrogate each space and estimate the
394 number of susceptible people infected in the Big Office, when an infected
395 person is present. The proportion of the susceptible population infected in

396 each space is given in Figure 4. It predicts that there were no transmissions
397 in 90% of the spaces. However, when a transmission does occur, the most
398 common outcome is a single transmission event. This indicates that the
399 dose inhaled by all susceptible people is usually small enough not to lead
400 to an infection. This is confirmed by Figure 5, which gives the cumulative
401 distribution of dose for both scenarios. It shows that susceptible occupants
402 receive no dose in Big Office spaces 61% of the time and 95% of the time in
403 Small Office spaces.

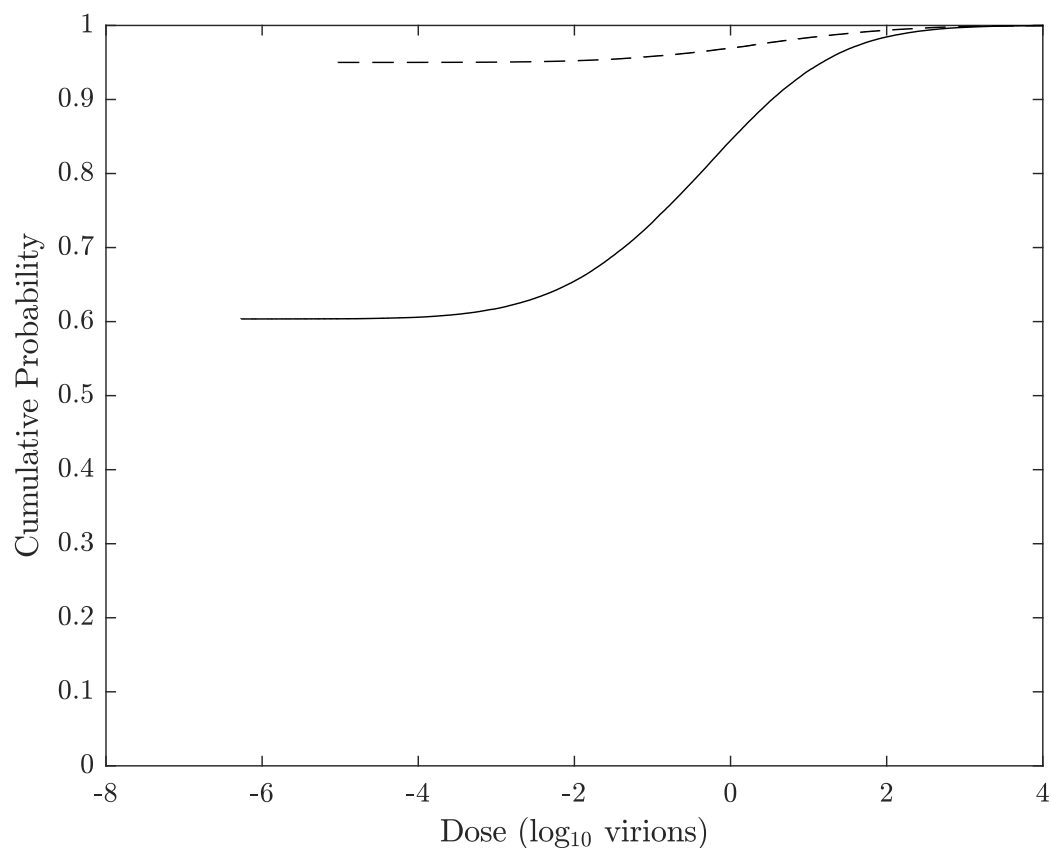


Figure 5: The cumulative probability of the dose in the Big Office (solid) and the Small Office (dashed) when $C = 1\%$.

404 More than 40 susceptible people are infected in the Big Office only 0.3%
405 of the time; see Figure 4. This suggests that so called *super-spreader* events
406 that occur by far-field airborne transmission alone, are likely to be rare. This
407 distribution reflects the overdispersion of transmission recorded for SARS-
408 CoV-2 and, although this work only considers one transmission route, similar
409 relationships between the viral load and the number of transmission events
410 may also be true for other transmission routes [11, 32, 33, 34, 35, 36, 37, 38].

411 Applying the MC approach to the Small Office shows that the overdispersion
412 is less pronounced because there are fewer susceptible people and fewer
413 infected people in each space. This limits the number of susceptible people
414 who can be infected when the viral load is high. Here, 0.2% of all spaces, and
415 22% of spaces with at least one transmission, had 4 infections of susceptible
416 people.

417 There are very few epidemiological examples of high secondary COVID-
418 19 transmission events where $> 80\%$ of occupants in a space are infected and
419 this suggests that our assumptions over-estimate the viral emission rate. One
420 reason is the assumption that all genome copies are viable virions, which is
421 very unlikely.

422 Figure 4 shows that the frequency of the number of susceptible people
423 infected is highest at zero and decreases as the number of susceptible people
424 infected increases. However, the frequency later increases as the number
425 of susceptible people infected approaches the number of occupants. This
426 reflects the shape of the probability of infection curve in Figure 2 where a
427 point is reached when the viral load leads to the infection of all susceptible
428 people, and a higher viral load cannot infect more people. The phenomena

429 is a function of occupancy and is less likely to occur as the number of occu-
430 pants increases because the viral load required to infect all susceptible people
431 increases, assuming that the *per capita* space volume and ventilation rate are
432 constant.

433 5.2. Ventilation and space volume

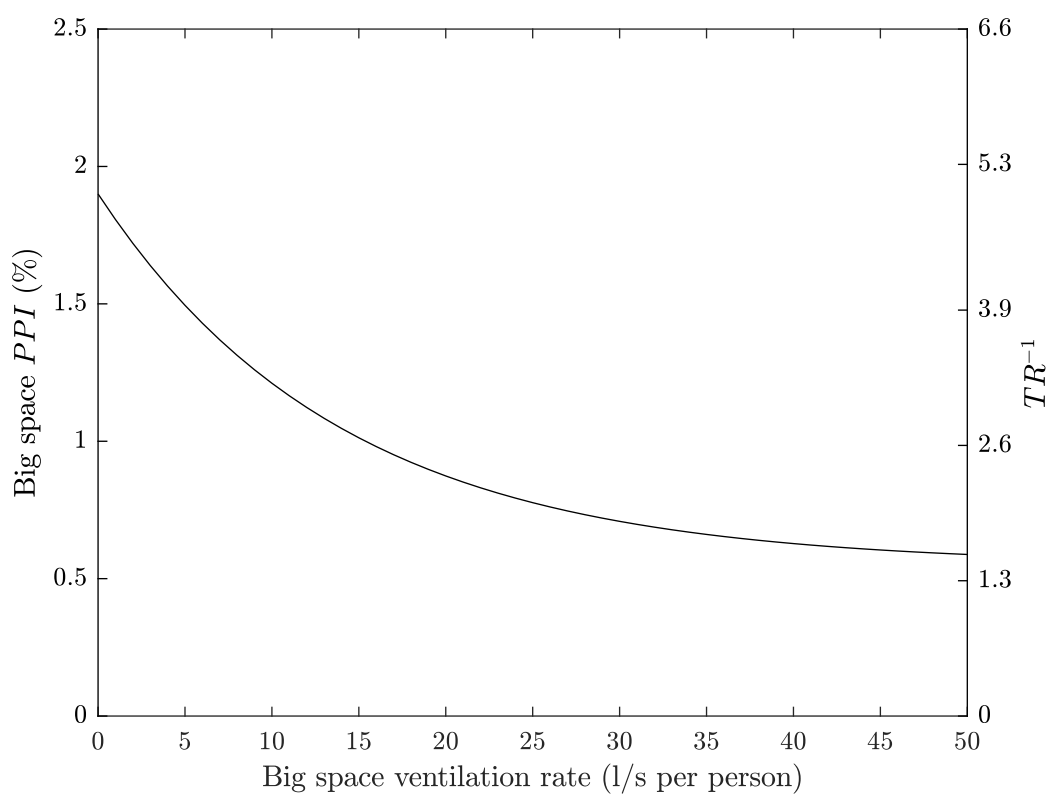


Figure 6: The effect of increasing the *per capita* ventilation rate, $\psi V N^{-1}$, in the Big Office on the *PPI* and the *TR* when the *per capita* ventilation rate in the Small Office is a constant 10l s^{-1} per person. All values are illustrative.

434 The quotient of the proportion of people infected in the two scenarios
435 gives a Transmission Ratio, *TR*, see Equation 14. Increasing the *per capita*
436 ventilation rate, $\psi V N^{-1}$, or space volume, $V N^{-1}$, in the Big Office reduces

437 the inverse of the TR . This has the effect of increasing the total removal rate,
438 ϕ , and reducing the dose and the probability of infection; see Equation 1 and
439 Figure 6. However, there is a law of diminishing returns in reducing the PPI
440 by increasing the ventilation rate because the dose is inversely proportional
441 to ϕ . Therefore, it is more important to increase the ventilation rate in a
442 poorly ventilated space than in a well ventilated space because the change in
443 the PPI is greater.

444 A similar effect is seen when increasing the *per capita* space volume in the
445 Big Office while maintaining a constant *per capita* ventilation in both spaces.
446 This is because the dose is inversely proportional to volume. Furthermore,
447 the product of the space volume and the total removal rate, ϕV , is propor-
448 tional to the concentration of the virus in the air and, therefore, the infectious
449 dose. The *per capita* ventilation rate is constant in both spaces and so the
450 air change rate in the Big Office decreases as its volume increases. However,
451 this reduction is offset by the surface deposition and biological decay rates,
452 which remain constant and have a greater effect on the value of the equivalent
453 ventilation rate, ψV , as the space volume increases; see Section 2.1.

454 Equation 1 assumes a steady-state concentration of the virus has been
455 reached based on the assumption that the exposure time, T , is significant.
456 However, the time taken to reach the steady-state concentration in large
457 spaces may be significant and affects the dose over shorter exposure periods.
458 This is an example of the *reservoir effect*, the ability of indoor air to act as
459 a fresh-air reservoir and absorb the impact of contaminant emissions. The
460 greater the space volume, the greater the effect. These factors highlight the
461 benefits of increasing the *per capita* space volume.

462 5.3. Occupancy

463 Figure 7 shows the effect of increasing the number of occupants in the
464 Big Office while maintaining both the *per capita* space volume, $V N^{-1}$, and
465 ventilation rate, $\psi V N^{-1}$. As the number of occupants increases, the *PPI*
466 increases at an ever diminishing rate because the magnitude of the equivalent
467 ventilation rate, ϕV , increases at a greater rate than the probability of the
468 mean number of infected people, \bar{I} .

469 However, if the volume and ventilation rate remain constant as the oc-
470 cupancy increases, Figure 8 shows that the *PPI* and the inverse of the *TR*
471 increase linearly with occupancy. Here, the total removal rate, ϕ , remains
472 constant but the *per capita* space volume and ventilation rate reduce. There-
473 fore, the Big Office could have 14 occupants and have the same *PPI* as the
474 Small Office occupied by 5 people. Extrapolating to two identical popula-
475 tions of 140 people split into 28 Small Offices with 5 people in each, and 10
476 Big Offices with 14 people in each, the same *PPI* can be achieved.

477 This suggests that reducing the number of occupants in a space is the
478 most effective means of reducing the inverse of *TR* towards unity. To achieve
479 the same goal by increasing the ventilation rate or the *per capita* space volume
480 would require unfeasibly large increases in both.

481 5.4. Community infection rate

482 Figure 9 shows that the community infection rate, C , has a significant ef-
483 fect on the *PPI* and the *TR*. This is because it affects both the probability of
484 an infectious level of viral load, $P(L)$, and the probability of having suscepti-
485 ble people in a space, $P(S)$; see Equation 10. When $C > 1\%$, the probability
486 of transmission increases dramatically, suggesting that it strongly influences

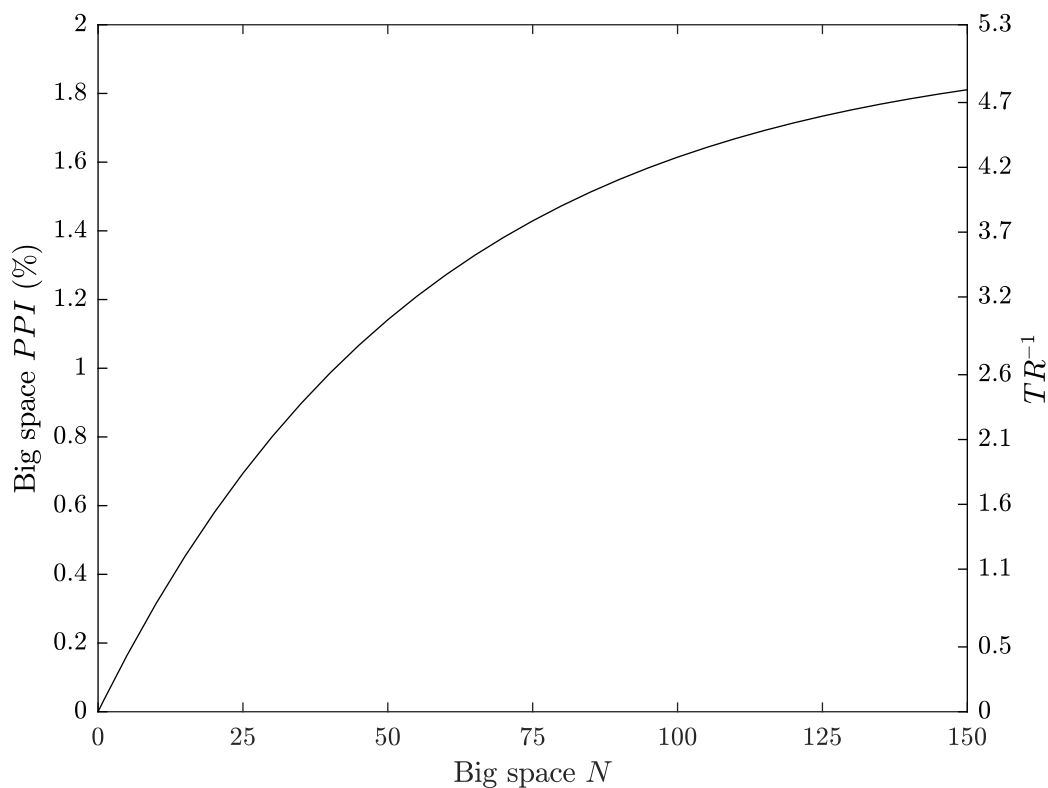


Figure 7: The effect of increasing the occupancy, N , in the Big Office, where the space volume per person and ventilation rate per person is fixed at 30 m^3 and 10 l s^{-1} respectively, on the PPI (green) and TR (black). All values are illustrative.

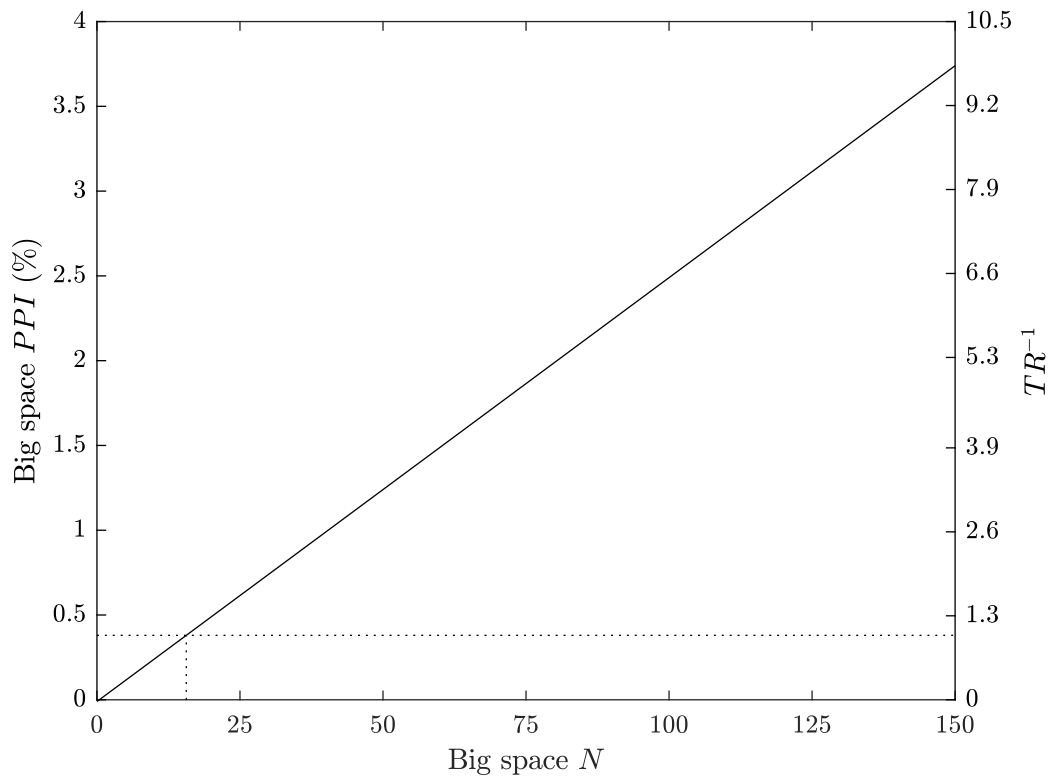


Figure 8: The effect of increasing the occupancy, N , in the Big Office where the space volume and ventilation flow rate are fixed for a designed occupancy of 50 people (1500 m^3 and 500 l s^{-1} , respectively), on the PPI and TR . All values are illustrative.

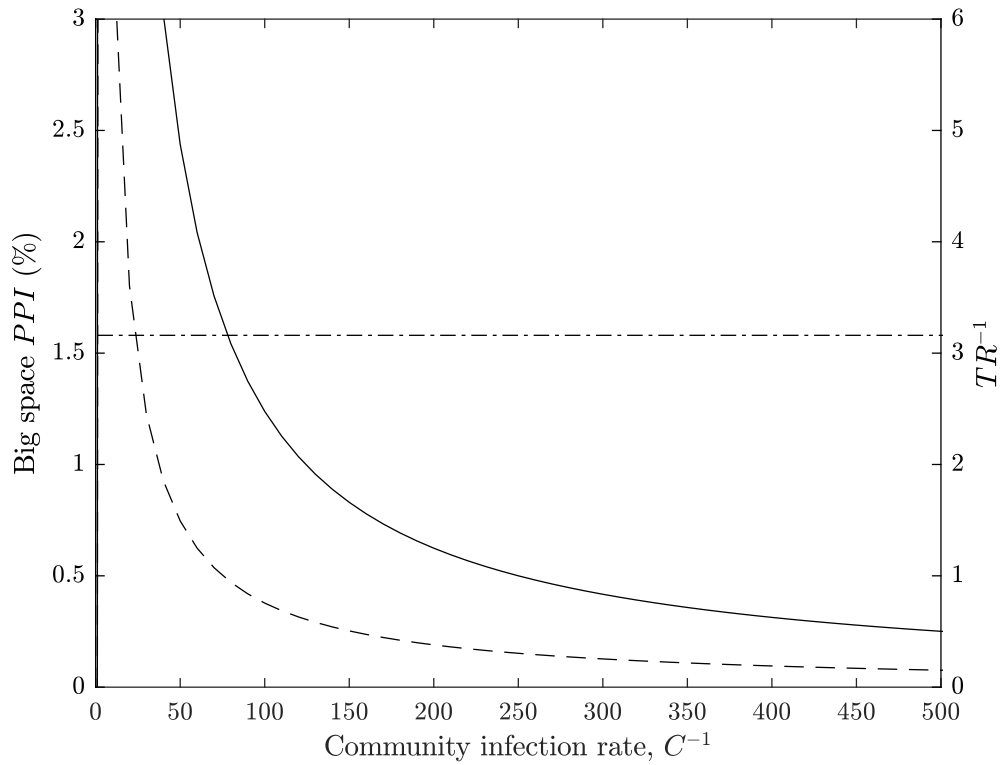


Figure 9: The effect of decreasing the community infection rate, C , on the PPI in the Big Office (solid) and the Small Office (dash) and on the TR (dot-dash). All values are illustrative.

487 the spread of the virus indoors. Figure 9 also shows that C only affects
488 the TR when the number of occupants, N , is less than the reciprocal of the
489 community infection rate in both spaces, $N < 1/C$. Thereafter, the TR is
490 constant irrespective of the community infection rate; see the Supplementary
491 Materials¹.

492 5.5. Limitations

493 Some limitations and uncertainties in this work have already been ad-
494 dressed, particularly those concerning the viral load and the dose-response
495 relationship. However, there are a number of other aspects that increase
496 uncertainty in it. Firstly, the models assume homogenous instantly mixed
497 indoor air to simplify the estimate of a dose. This assumption is unlikely to
498 be true in some spaces, especially in large spaces where the concentrations of
499 virions in the air is likely be a function of the distance from the infected per-
500 son, although it is unclear at which space volume this assumption becomes
501 less useful[39].

502 The approach described in Section 2 only considers the far-field trans-
503 mission of virus, and not near-field transmission, which is likely to be the
504 dominant route of transmission. The concentration of the virus in aerosols
505 and droplets per unit volume of air is several orders of magnitude greater
506 closer to the infected person at distances of < 2 m [3, 9]. However, it is likely
507 that the method of calculating the probability of viral load of infected people,
508 $P(L)$, is also important for the dose received by near-field transmission and
509 should be explored further in the future.

510 The distribution of viral load of an infected person around the median
511 will affect the probability of transmission. We apply a normal distribution

512 of \log_{10} values, see Section 2, but another, such as the Weibull distribution,
513 will affect the transmission probabilities differently.

514 The model also assumes a naïve population of susceptible people, and it
515 is unclear whether a higher infectious dose is required for susceptible people
516 who have a greater immune response obtained from vaccination or a previous
517 infection. It also assumes everyone is equally susceptible, which is unlikely.
518 This paper does not consider the effect of the magnitude of the dose on
519 subsequent disease severity. However, a recent review suggests that it is
520 highly unlikely there is a link between dose and disease severity [40].

521 There is uncertainty in the dose-response relationship and the propor-
522 tion of people infected. In the absence of knowledge, we have assumed that
523 the dose-response curve for SARS-CoV-1 also applies to SARS-CoV-2; see
524 Section 2.1. The SARS-CoV-1 dose-response curve was generated from four
525 groups of inoculated transgenic mice [23] that were genetically modified to
526 express the human protein receptor of the SARS-CoV-1 virus. In three of the
527 groups all mice were infected and in the fourth one-third were infected. The
528 dose-response curve was fitted to data from these four groups and, although
529 it is limited, it is sufficient to assume that the curve follows the exponential
530 distribution rather than the Beta-Poisson distribution. A further limitation is
531 that the response of humans to a dose of SARS-CoV-1 may vary significantly
532 from that of transgenic mice. For a further discussion, see the Supplemental
533 Material¹. There is also uncertainty in the measurement of the viral load
534 used to challenge the study, and whether or not dose curves are valid for
535 predicting low probabilities of infection at very low virus titres. Other stud-
536 ies have used alternative dose-response curves for other coronaviruses, all

537 of which have similar uncertainties [21, 16], but this framework provides a
538 means to test other dose-response relationships by adjusting k in Equation 1.

539 The viral load of an infected person is the number of RNA copies ml^{-1} of
540 respiratory fluid, whereas the viral emission is the amount of RNA copies per
541 unit volume of exhaled breath; see Section 2.1. It has been established that
542 the viral load of an infected person increases in time from the moment of
543 infection and is highest just before, or at, the onset of COVID-19 symptoms.
544 As COVID-19 progresses the viral load reduces, normally within the first
545 week after the onset of symptoms [41, 42]. The viral load also varies between
546 people at any stage of the infection, which increases uncertainty in it [43, 44,
547 45, 19, 46, 18, 30, 37, 47].

548 The viral load can be inferred from the *cycle threshold* values of real time
549 reverse transcription quantitative polymerase chain reaction (RT qPCR) na-
550 sopharyngeal (NP) swabs. This method assumes a direct correlation be-
551 tween the viral load of a swab and the viral load of respiratory fluid [48, 12].
552 RT qPCR is a semi-quantitative method because it requires a number of
553 amplification cycles to provide a positive signal of the SARS-CoV-2 genome,
554 which is proportional to the initial amount of viral genome in the original
555 sample. The cycle threshold is the number of polymerase chain reaction
556 cycles that are required before the chemical luminescence is read by the
557 equipment. The lower the starting amount of viral genome, the greater the
558 number of amplification cycles required. A calibrated standard curve is then
559 used to estimate the starting amount of viral genomic material. However,
560 the standard curve varies between test assays (investigative procedures) and
561 different RT qPCR thermal cyclers, the laboratory apparatus used to amplify

562 segments of RNA. This method also assumes a complete doubling of genetic
563 material after each cycle. The exponential relationship means that errors
564 in the calculation of the initial quantity of genomic material are orders of
565 magnitude higher for low cycle counts than for high cycle counts. Addition-
566 ally, if genomic data is taken from NP swabs, the estimated concentration of
567 genomic material per unit volume is often related to the amount of genomic
568 material in the buffer solution² in which NP swabs are eluted and used in
569 the assay, and not necessarily to the amount in a patient's respiratory fluid.
570 The amount of genomic material added to the buffer solution is dependent
571 on both a patient's viral load and the quality of the collection of the NP
572 sample, which is highly variable. Therefore, it is not possible to determine
573 absolute values of the viral load in a patient's respiratory fluid using this
574 method. However, data collected in this way is indicative of a range of vari-
575 ability, much of which is likely to be proportional to the viral load of the
576 person at the time the sample was collected. Some recent data suggests that
577 the viral load of NP swabs may not reflect the amount of infectious material
578 present [19]. However, it is important to note that there are wide variations
579 in the measured genomic material in NP swabs and that the viral load in
580 respiratory fluid is likely to vary by several orders of magnitude.

581 There is clearly uncertainty in the viral load of respiratory fluid. There is
582 also uncertainty in the viral concentration in respiratory aerosols and droplets
583 and the distribution is currently unclear. Some studies suggest that the
584 number of virions in small aerosols with a diameter of $< 1 \mu\text{m}$ is higher

²A *buffer solution* resists a change in its pH when a small quantity of acid or alkali is added to it

585 than would be expected given the viral concentration in the respiratory fluid
586 [49, 50] and that for SARS-CoV-2 there may be more genomic material in
587 the smallest aerosols [51].

588 There is high variability between people in the total volume of aerosols
589 generated per unit volume of exhaled breath, and it is dependent upon the
590 respiratory activity, such as talking and singing, and the respiratory capacity
591 [52, 53, 54, 55]. Coleman *et al.* [51] show that SARS-CoV-2 genomic material
592 is detectable in expired aerosols from *some* COVID-19 patients, but not all
593 of them because 41% exhaled no detectable genomic material. Singing and
594 talking generally produce more genomic material than breathing, but there
595 is large variability between patients. This suggests that respiratory activities
596 that have previously been shown to increase aerosol mass also increase the
597 amount of viral genomic material emitted. However, the viral concentration
598 in aerosols cannot be determined because the study did not measure the
599 mass of aerosols generated. Coleman *et al.* also show that the variability in
600 the amount of genomic material measured in expired aerosols is consistent
601 with the variability of viral loads determined using swabs and saliva [51].

602 Similarly, Adenaiye *et al.* [56] detected genomic material in aerosols from
603 patients infected with SARS-CoV-2 who provided a sample of exhaled air
604 when talking or singing. Genomic material was more frequently detected
605 in exhaled aerosols when the viral load of saliva or mid-turbinate swabs
606 was high; $> 10^8$ and $> 10^6$ RNA copies for mid-turbinate swabs and saliva
607 samples, respectively. Furthermore, they were able to culture viable virus
608 from $< 2\%$ of fine aerosol samples. It should be noted that one positive
609 sample was from a culture obtained from a fine aerosol sample that had an

610 amount of genomic material that was less than the detection limit of the
611 qRT PCR method, so it could be an artefact. Nevertheless, this provides
612 some evidence to support the epidemiological evidence that viable virus can
613 exist in exhaled aerosols.

614 Miller *et al.* suggests that around 1 : 1000 genome copies are likely to be
615 infectious virion [57, 12]. Adenaiye *et al.* use mid-turbinate swabs to estimate
616 that there are around 1 : 10⁴ viable virus per measured genome copies[56].
617 We make the assumption that all genome copies are viable virion, which
618 either over-estimates their infectiousness when using the Coleman *et al.* data,
619 or is similar to the assumption of Miller *et al.* if the viable virion emission
620 rate (calculated from air in a hospital) is in the order of 1000 virions per hour;
621 see Appendix A.

622 **6. Conclusions**

623 The number of occupants in a space can influence the risk of far-field air-
624 borne transmission that occurs at distances of > 2 m because the likelihood of
625 having infectious and susceptible people are both associated with the number
626 of occupants. Therefore, mass-balance and dose-response models are applied
627 to determine if it is advantageous to sub-divide a large reference space into
628 a number of identical smaller comparator spaces to reduce the transmission
629 risk for an individual person and for a population of people.

630 The reference space is an office with a volume of 1500 m³ occupied by
631 50 people over an 8 hour period, and has a ventilation rate of 10 l s⁻¹ per per-
632 son. The comparator space is occupied by 5 people and preserves the oc-
633 cupancy period and the *per capita* volume and ventilation rate. The dose

634 received by an individual susceptible person in the comparator Small Office,
635 when a single infected person is present, is compared to that in the reference
636 Big Office for the same circumstances to give a relative exposure index (REI)
637 with a value of 10 in the Small Office. This REI is a measure of the risk of
638 a space relative to the geometry, occupant activities, and exposure times of
639 the reference scenario and so it is not a measure of the probability of infec-
640 tion. Accordingly, when a single infected person is assumed to be present, a
641 space with more occupants is less of a risk for susceptible people because the
642 equivalent ventilation rate per infected person is higher.

643 The assumption that only one infected person is present is clearly prob-
644 lematic because, for a community infection rate of 1%, the most likely num-
645 ber of infected people in a 50 person space is zero. A transmission event
646 can only occur when there are both one or more infected people present in
647 a space and one or more susceptible people are present. The probability of
648 a transmission event occurring increases with the number of occupants and
649 the community infection rate; for example, the Big Office is over 12 times
650 more likely to have infected people present than the Small Office. However,
651 the geometry and ventilation rate in a larger space are non-linearly related to
652 the number of infected and susceptible people and so their relationship with
653 the probability of a transmission event occurring is also non-linear. These
654 effects are evaluated by considering a large population of people. But, this
655 introduces uncertainty in factors that vary across the population, such as the
656 viral load of an infected person, defined as the number of RNA copies ml^{-1}
657 of respiratory fluid. The viral load varies over time and between people at
658 any stage of the infection.

659 By applying a distribution of viral loads across a population of infected
660 people, secondary transmissions (new infections) are found to be likely to
661 occur only when the viral load is high, which agrees with Schijven *et al.*[38],
662 although the probabilities of this occurring in the Big Office and the Small
663 Office are low. This makes it hard to distinguish the route of transmission
664 epidemiologically. Generally, the viral load must be greater in the Big Office
665 than in the Small Office to achieve the same proportion of the population
666 infected when the community infection rate is $\leq 1\%$. The viable fraction is
667 unknown but a value of unity was chosen for computational ease, yet the esti-
668 mated doses and infection probabilities are small. Therefore, it is likely that
669 far-field transmission is a rare event that requires a high emission rate and
670 that there is a set of Goldilocks conditions that are *just right* where ventila-
671 tion is an effective mitigation method against transmission. These conditions
672 depend on the viral load, because when it is low or high, ventilation has little
673 effect on the risk of transmission.

674 There are circumstances where the magnitude of the total viral load of the
675 infected people is too high to affect the probability of secondary transmissions
676 by increasing ventilation and space volume. Conversely, when the total viral
677 load is very small, the dose is so small that it is highly unlikely to lead
678 to an infection in any space irrespective of its geometry or the number of
679 susceptible people present. There is a law of depreciating returns for the dose
680 and, therefore, the probability of infection, and the ventilation rate because
681 they are inversely related. Accordingly, it is better to focus on increasing
682 effective ventilation rates in under-ventilated spaces rather than increasing
683 ventilation rates above those prescribed by standards, or increasing effective

684 ventilation rates using air cleaners, in already well-ventilated spaces.

685 There are significant uncertainties in the modelling assumptions and the
686 data used in the analysis and it is not possible to have confidence in the calcu-
687 lated magnitudes of doses or the proportions of people infected. However, the
688 general trends and relationships described herein are less uncertain and may
689 also apply to airborne pathogens other than SARS-CoV-2 at the population
690 scale. Accordingly, it is possible to say that there are benefits of subdivid-
691 ing a population, but their magnitudes need to be considered against other
692 factors, such as the overall working environment, labour and material costs,
693 and inadvertent changes to the ventilation system and strategy. However,
694 it is likely that the benefits do not outweigh the costs in existing buildings
695 when a less conservative viable fraction or a lower community infection rate
696 is used because it decreases the magnitude of the benefits significantly. It is
697 likely to be more cost-effective to consider the advantages of partition when
698 designing new resilient buildings because the consequences can be considered
699 from the beginning.

700 There are other factors that will reduce the risk of transmission in ex-
701 isting buildings. Local and national stakeholders can seek to maintain low
702 community infection rates, detect infected people with high viral loads us-
703 ing rapid antigen tests and support to isolate them (see the Supplementary
704 Materials¹), reduce the variance and magnitude of the viral load in a popu-
705 lation by encouraging vaccination [30]. Changes can be made to the use of
706 existing buildings and their services, such as reducing the occupancy density
707 of a space below the level it was designed for while preserving the magnitude
708 of the ventilation rate, reducing exposure times, and ensuring compliance

709 with ventilation standards.

710 **Acknowledgements**

711 The authors acknowledge the Engineering and Physical Sciences Research
712 Council (EP/W002779/1) who financially supported this work. They are also
713 grateful to Constanza Molina for her comments on this paper.

714 **Appendix A. Estimating viral emission from viral load**

715 We assume that the RNA copies ml^{-1} concentration is constant in aerosols
716 and in NP swabs and then we use the assumptions of Jones *et al.* [15] to con-
717 vert a NP viral load into a virus emission rate. This method follows Jones *et*
718 *al.* and is derived from the work of Morawskwa *et al.* who determine vol-
719 ume distribution aerosols for different respiratory activities, and is similar
720 to that used by Lelieveld *et al.* [15, 17, 55]. Table A.3 shows the estimated
721 virus emission rate for different respiratory activities when the viral load is
722 10^7 RNA copies ml^{-1} . For comparison, median measured values of virus emis-
723 sion in aerosols from Coleman *et al.* are given. These values were measured
724 by collecting RNA copies from COVID-19 patients, where the median cycle
725 threshold, required to process diagnostic samples, was 16. [51].

726

Table A.3: Estimated emission rates from an infected person with a viral load of 10^7 RNA copies ml^{-1} compared to measured emission rates from patients with a median cycle threshold of 16 [51]

	Estimated RNA copies h^{-1}	Measured median RNA copies h^{-1}
Breathing	203	127
Voiced counting (talking)	967	1912
Vocalisation (singing)	6198	2856
Breathing:talking 25:75	394	573*

*calculated using measured values for breathing and talking.

727 Additionally, unpublished work by Adenaiye *et al.* measured viral genome
728 in patients infected by the SARS-CoV-2 alpha variant, who were breathing
729 and talking, in coarse ($> 5 \mu\text{m}$) and fine ($\leq 5 \mu\text{m}$) aerosols with a total geo-
730 metric mean of 1440 RNA copies h^{-1} and a maximum of 3×10^5 RNA copies h^{-1}
731 [56]. These are greater than the estimated values given in Table A.3, but the
732 viral load, measured by genome copies from mid-turbinate swabs, was gen-
733 erally orders of magnitude higher than 10^7 RNA copies ml^{-1} .

734 In Section 4, the inhaled dose is calculated for all possible viral loads.
735 Here, it should be noted that the calculated RNA copies emission rate is as-
736 sumed to be linearly related to the viral load of respiratory fluids, so that a vi-
737 ral load of 10^8 RNA copies ml^{-1} has a ten-fold greater emission rate. For com-
738 parison, a virus emission rate of 394 RNA copies h^{-1} (assumed for a viral load
739 of 10^7 RNA copies ml^{-1}) leads to individual doses of around 2.2 RNA copies
740 and 0.2 RNA copies for the Small Office and Big Office scenarios, respectively.

741 The calculated emission rate of viral genome for a viral load of 10^7 RNA copies ml^{-1}

742 is a reasonable fit to the Coleman *et al.* and Adenaiye *et al.* data. For further
743 details see the Supplementary Materials¹.

744 **Appendix B. Pseudocode**

```
745 SET population size
746 SET scenario space volumes
747 SET scenario people per space
748 FOR each scenario
749     COMPUTE number of spaces
750     FOR each space
751         SAMPLE infected people from binomial distribution
752         IF infected people is number of occupants THEN
753             SET infected people to zero
754         END IF
755         COMPUTE susceptible & exposed people
756         IF infected people is zero THEN
757             SET susceptible & exposed people to zero
758         END IF
759         SAMPLE log10 viral load from normal distribution
760         COMPUTE emission rate using viral load
761         COMPUTE dose using emission rate
762         COMPUTE probability of infection per susceptible person
763         SAMPLE infected susceptible people from binomial distribution
764     END FOR
765     COMPUTE number of transmission events
```

```
766     COMPUTE probability of infected people present
767     COMPUTE individual probability being susceptible & exposed
768     COMPUTE mean number of infected people
769     COMPUTE mean emission rate
770     COMPUTE mean dose
771     COMPUTE mean probability of infection
772     COMPUTE proportion of population infected
773 END FOR
774 COMPUTE transmission ratio
```

775 **References**

- 776 [1] C. C. Wang, K. A. Prather, J. Sznitman, J. L. Jimenez, S. S. Lakdawala,
777 Z. Tufekci, L. C. Marr, Airborne transmission of respiratory viruses, *Sci-*
778 *ence* 373 (6558) (2021) eabd9149. doi:10.1126/science.abd9149.
779 URL [https://www.sciencemag.org/lookup/doi/10.1126/science.](https://www.sciencemag.org/lookup/doi/10.1126/science.abd9149)
780 [abd9149](https://www.sciencemag.org/lookup/doi/10.1126/science.abd9149)
- 781 [2] L. Bourouiba, Turbulent Gas Clouds and Respiratory Pathogen Emis-
782 sions: Potential Implications for Reducing Transmission of COVID-19,
783 *JAMA - Journal of the American Medical Association* 323 (18) (2020)
784 1837–1838. doi:10.1001/jama.2020.4756.
- 785 [3] G. Cortellessa, L. Stabile, F. Arpino, D. Faleiros, W. van den Bos,
786 L. Morawska, G. Buonanno, Close proximity risk assessment for SARS-
787 CoV-2 infection, *Science of The Total Environment* 794 (2021) 148749.
788 doi:10.1016/j.scitotenv.2021.148749.
789 URL <https://doi.org/10.1016/j.scitotenv.2021.148749>
- 790 [4] Q. Yang, T. K. Saldi, P. K. Gonzales, E. Lasda, C. J. Decker, K. L.
791 Tat, M. R. Fink, C. R. Hager, J. C. Davis, C. D. Ozeroff, D. Muhrad,
792 S. K. Clark, W. T. Fattor, N. R. Meyerson, C. L. Paige, A. R. Gilchrist,
793 A. Barbachano-Guerrero, E. R. Worden-Sapper, S. S. Wu, G. R. Bris-
794 son, M. B. McQueen, R. D. Dowell, L. Leinwand, R. Parker, S. L.
795 Sawyer, Just 2 percent of sars-cov-2 positive individuals carry 90 per-
796 cent of the virus circulating in communities, *Proceedings of the National*
797 *Academy of Sciences* 118 (21) (2021) e2104547118. doi:10.1073/pnas.

798 2104547118.

799 URL <http://www.pnas.org/lookup/doi/10.1073/pnas.2104547118>

800 [5] P. Dabisch, M. Schuit, A. Herzog, K. Beck, S. Wood, M. Krause,
801 D. Miller, W. Weaver, D. Freeburger, I. Hooper, B. Green, G. Williams,
802 B. Holland, J. Bohannon, V. Wahl, J. Yolitz, M. Hevey, S. Ratnesar-
803 Shumate, The influence of temperature, humidity, and simulated sun-
804 light on the infectivity of SARS-CoV-2 in aerosols, *Aerosol Science*
805 *and Technology* 55 (2) (2021) 142–153. doi:10.1080/02786826.2020.
806 1829536.

807 URL [https://www.tandfonline.com/doi/full/10.1080/02786826.](https://www.tandfonline.com/doi/full/10.1080/02786826.2020.1829536)
808 2020.1829536

809 [6] Z. Liu, Q. Guo, L. Zou, H. Zhang, M. Zhang, F. Ouyang, J. Su, W. Su,
810 J. Xu, H. Lin, J. Sun, J. Peng, H. Jiang, P. Zhou, H. Zhen, T. Liu,
811 R. Che, H. Zeng, Z. Zheng, J. Yu, L. Yi, J. Wu, J. Chen, H. Zhong,
812 X. Deng, M. Kang, O. G. Pybus, M. Hall, K. A. Lythgoe, Viral infection
813 and transmission in a large well- traced outbreak caused by the Delta
814 SARS-CoV-2 variant, *Virological.org* (2021).

815 URL <https://virological.org/t/viral-infection-and-transmission-in-a-large-wel>
816 724

817 [7] T. C. Bulfone, M. Malekinejad, G. W. Rutherford, N. Razani, Out-
818 door Transmission of SARS-CoV-2 and Other Respiratory Viruses: A
819 Systematic Review, *The Journal of infectious diseases* 223 (4) (2021)
820 550–561. doi:10.1093/infdis/jiaa742.

821 [8] M. Weed, A. Foad, Rapid scoping review of evidence of outdoor trans-

- 822 mission of COVID-19, (pre-print) (2020). doi:10.1101/2020.09.04.
823 20188417.
- 824 [9] N. Zhang, W. Chen, P. T. Chan, H. L. Yen, J. W. T. Tang, Y. Li, Close
825 contact behavior in indoor environment and transmission of respiratory
826 infection, *Indoor Air* 30 (4) (2020) 645–661. doi:10.1111/ina.12673.
- 827 [10] SAGE, SARS-COV-2 Transmission routes and environments, Tech.
828 Rep. October, SAGE, UK (2020).
829 URL [https://assets.publishing.service.gov.uk/government/
830 uploads/system/uploads/attachment_data/file/933225/S0824_
831 SARS-CoV-2_Transmission_routes_and_environments.pdf](https://assets.publishing.service.gov.uk/government/uploads/system/uploads/attachment_data/file/933225/S0824_SARS-CoV-2_Transmission_routes_and_environments.pdf)
- 832 [11] K. Escandón, A. L. Rasmussen, I. I. Bogoch, E. J. Murray, K. Es-
833 candón, S. V. Popescu, J. Kindrachuk, COVID-19 false dichotomies
834 and a comprehensive review of the evidence regarding public health,
835 COVID-19 symptomatology, SARS-CoV-2 transmission, mask wear-
836 ing, and reinfection, *BMC Infectious Diseases* 21 (1) (2021) 710.
837 arXiv:arXiv:1011.1669v3, doi:10.1186/s12879-021-06357-4.
838 URL [https://osf.io/k2d84/https://bmcinfectdis.
839 biomedcentral.com/articles/10.1186/s12879-021-06357-4](https://osf.io/k2d84/https://bmcinfectdis.biomedcentral.com/articles/10.1186/s12879-021-06357-4)
- 840 [12] S. L. Miller, W. W. Nazaroff, J. L. Jimenez, A. Boerstra, S. J. Dancer,
841 J. Kurnitski, L. C. Marr, L. Morawska, C. Noakes, Transmission of
842 SARS-CoV-2 by inhalation of respiratory aerosol in the Skagit Valley
843 Chorale superspreading event, *Indoor Air* in press (2020). doi:doi.
844 org/10.1111/ina.12751.

- 845 [13] D. Hijnen, A. Marzano, K. Eyerich, C. GeurtsvanKessel, A. Giménez-
846 Arnau, P. Joly, C. Vestergaard, M. Sticherling, E. Schmidt, Sars-cov-2
847 transmission from presymptomatic meeting attendee, germany., *Emerg-*
848 *ing infectious diseases* 26 (8) (2020). doi:10.3201/eid2608.201235.
- 849 [14] L. M. Groves, L. Usagawa, J. Elm, E. Low, A. Manuzak, J. Quint, K. E.
850 Center, A. M. Buff, S. K. Kemble, Community Transmission of SARS-
851 CoV-2 at Three Fitness Facilities — Hawaii, June–July 2020, *MMWR*
852 *Surveillance Summaries* 70 (9) (2021) 316–320. doi:10.15585/mmwr.
853 mm7009e1.
- 854 [15] B. Jones, P. Sharpe, C. Iddon, E. A. Hathway, C. J. Noakes, S. Fitzger-
855 ald, Modelling uncertainty in the relative risk of exposure to the SARS-
856 CoV-2 virus by airborne aerosol transmission in well mixed indoor air,
857 *Building and Environment* 191 (October 2020) (2021) 107617. doi:
858 10.1016/j.buildenv.2021.107617.
859 URL <https://doi.org/10.1016/j.buildenv.2021.107617>
- 860 [16] H. Parhizkar, K. G. Van Den Wymelenberg, C. N. Haas, R. L. Corsi, A
861 Quantitative Risk Estimation Platform for Indoor Aerosol Transmission
862 of COVID-19, *Risk Analysis* 0 (0) (2021). doi:10.1111/risa.13844.
- 863 [17] J. Lelieveld, F. Helleis, S. Borrmann, Y. Cheng, F. Drewnick, G. Haug,
864 T. Klimach, J. Sciare, H. Su, U. Pöschl, Model calculations of aerosol
865 transmission and infection risk of covid-19 in indoor environments, *Inter-*
866 *national Journal of Environmental Research and Public Health* 17 (21)
867 (2020) 1–18. doi:10.3390/ijerph17218114.

- 868 [18] P. Z. Chen, N. Bobrovitz, Z. Premji, M. Koopmans, D. N. Fisman, F. X.
869 Gu, Heterogeneity in transmissibility and shedding SARS-CoV-2 via
870 droplets and aerosols, *eLife* 10 (2021) 1–32. doi:10.7554/eLife.65774.
- 871 [19] R. Ke, P. P. Martinez, R. L. Smith, L. L. Gibson, A. Mirza, M. Conte,
872 N. Gallagher, C. H. Luo, J. Jarrett, A. Conte, M. Farjo, K. K. O.
873 Walden, G. Rendon, C. J. Fields, R. Fredrickson, D. C. Edmonson,
874 M. E. Baughman, K. K. Chiu, J. Yedetore, J. Quicksall, A. N.
875 Owens, J. Broach, Daily sampling of early SARS-CoV-2 infection
876 reveals substantial heterogeneity in infectiousness, (pre-print) (2021).
877 doi:<https://doi.org/10.1101/2021.07.12.21260208>.
878 URL [https://www.medrxiv.org/content/10.1101/2021.07.12.](https://www.medrxiv.org/content/10.1101/2021.07.12.21260208v1)
879 [21260208v1](https://www.medrxiv.org/content/10.1101/2021.07.12.21260208v1)
- 880 [20] P. Z. Chen, N. Bobrovitz, Z. Premji, M. Koopmans, D. N. Fisman, F. X.
881 Gu, Sars-cov-2 shedding dynamics across the respiratory tract, sex, and
882 disease severity for adult and pediatric covid-19, *eLife* 10 (2021) e70458.
883 doi:10.7554/eLife.70458.
884 URL <https://doi.org/10.7554/eLife.70458>
- 885 [21] T. Watanabe, T. A. Bartrand, M. H. Weir, T. Omura, C. N. Haas,
886 Development of a dose-response model for sars coronavirus. risk analysis:
887 an official publication of the society for risk analysis, *Risk Anal* 30 (7)
888 (2010) 1129–1138. doi:10.1111/j.1539-6924.2010.01427.x.
- 889 [22] X. Zhang, J. Wang, Dose-response Relation Deduced for Coronaviruses
890 From Coronavirus Disease 2019, Severe Acute Respiratory Syndrome,
891 and Middle East Respiratory Syndrome: Meta-analysis Results and its

892 Application for Infection Risk Assessment of Aerosol Transmission, Clin-
893 ical Infectious Diseases 73 (1) (2020) 1–5. doi:10.1093/cid/ciaa1675.

894 [23] M. L. DeDiego, L. Pewe, E. Alvarez, M. T. Rejas, S. Perlman, L. En-
895 juanes, Pathogenicity of severe acute respiratory coronavirus deletion
896 mutants in hacc-2 transgenic mice, Virology 376 (2) (2008) 379–389.
897 doi:<https://doi.org/10.1016/j.virol.2008.03.005>.

898 URL [https://www.sciencedirect.com/science/article/pii/](https://www.sciencedirect.com/science/article/pii/S004268220800175X)
899 [S004268220800175X](https://www.sciencedirect.com/science/article/pii/S004268220800175X)

900 [24] SAGE, Emg: Role of ventilation in controlling sars-cov-2 transmission,
901 Tech. Rep. September, SAGE, UK (2020).

902 URL [https://www.gov.uk/government/publications/](https://www.gov.uk/government/publications/emg-role-of-ventilation-in-controlling-sars-cov-2-transmission-30-september-2020)
903 [emg-role-of-ventilation-in-controlling-sars-cov-2-transmission-30-september-2020](https://www.gov.uk/government/publications/emg-role-of-ventilation-in-controlling-sars-cov-2-transmission-30-september-2020)

904 [25] C. Molina, C. Iddon, P. Sharpe, B. Jones, CIBSE relative exposure
905 index calculator (2021).

906 URL [https://www.cibse.org/coronavirus-covid-19/](https://www.cibse.org/coronavirus-covid-19/emerging-from-lockdown#5)
907 [emerging-from-lockdown#5](https://www.cibse.org/coronavirus-covid-19/emerging-from-lockdown#5)

908 [26] P. Y. Chia, S. W. X. Ong, C. J. Chiew, L. W. Ang, J.-M. Chavatte,
909 T.-M. Mak, L. Cui, S. Kalimuddin, W. N. Chia, C. W. Tan, L. Y. A.
910 Chai, S. Y. Tan, S. Zheng, R. T. P. Lin, L. Wang, Y.-S. Leo, V. J. Lee,
911 D. C. Lye, B. E. Young, Virological and serological kinetics of sars-cov-
912 2 delta variant vaccine-breakthrough infections: a multi-center cohort
913 study, (pre-print) (2021).

914 [27] A. Singanayagam, S. Hakki, J. Dunning, K. J. Madon, M. A. Crone,

- 915 A. Koycheva, N. Derqui-Fernandez, J. L. Barnett, M. G. Whitfield,
916 R. Varro, A. Charlett, R. Kundu, J. Fenn, J. Cutajar, V. Quinn,
917 E. Conibear, W. Barclay, P. S. Freemont, G. P. Taylor, S. Ahmad,
918 M. Zambon, N. M. Ferguson, A. Lalvani, A. Badhan, S. Dustan,
919 C. Tejpal, A. V. Ketkar, J. S. Narean, S. Hammett, E. McDermott,
920 T. Pillay, H. Houston, C. Luca, J. Samuel, S. Bremang, S. Evetts,
921 J. Poh, C. Anderson, D. Jackson, S. Miah, J. Ellis, A. Lackenby,
922 Community transmission and viral load kinetics of the SARS-CoV-2
923 delta (B.1.617.2) variant in vaccinated and unvaccinated individuals in
924 the UK: a prospective, longitudinal, cohort study, *The Lancet Infectious*
925 *Diseases* 3099 (21) (oct 2021). doi:10.1016/S1473-3099(21)00648-4.
926 URL [https://linkinghub.elsevier.com/retrieve/pii/
927 S1473309921006484](https://linkinghub.elsevier.com/retrieve/pii/S1473309921006484)
- 928 [28] D. W. Eyre, D. Taylor, M. Purver, D. Chapman, T. Fowler, K. Pouwels,
929 A. S. Walker, T. E. A. Peto, The impact of SARS-CoV-2 vaccination
930 on Alpha and Delta variant transmission, (pre-print) (2021).
931 URL [http://medrxiv.org/content/early/2021/09/29/2021.09.
932 28.21264260.abstract](http://medrxiv.org/content/early/2021/09/29/2021.09.28.21264260.abstract)
- 933 [29] M. Cevik, S. D. Baral, Networks of SARS-CoV-2 transmission., *Science*
934 (New York, N.Y.) 373 (6551) (2021) 162–163. doi:10.1126/science.
935 abg0842.
936 URL <http://www.ncbi.nlm.nih.gov/pubmed/34244400>
- 937 [30] L. Y. W. Lee, S. Rozmanowski, M. Pang, A. Charlett, C. Anderson,
938 G. J. Hughes, M. Barnard, L. Peto, R. Vipond, A. Sienkiewicz,

939 S. Hopkins, J. Bell, D. W. Crook, N. Gent, A. S. Walker, T. E. A.
940 Peto, D. W. Eyre, Severe Acute Respiratory Syndrome Coronavirus
941 2 (SARS-CoV-2) Infectivity by Viral Load, S Gene Variants and
942 Demographic Factors, and the Utility of Lateral Flow Devices to
943 Prevent Transmission, *Clinical Infectious Diseases* 6 (2021) 1–32.
944 doi:10.1093/cid/ciab421.
945 URL [https://academic.oup.com/cid/advance-article/doi/10.](https://academic.oup.com/cid/advance-article/doi/10.1093/cid/ciab421/6273394)
946 [1093/cid/ciab421/6273394](https://academic.oup.com/cid/advance-article/doi/10.1093/cid/ciab421/6273394)

947 [31] ONS, ONS Coronavirus (COVID-19) Infection Survey,
948 [https://www.ons.gov.uk/peoplepopulationandcommunity/healthandsocialcare/conditionsand](https://www.ons.gov.uk/peoplepopulationandcommunity/healthandsocialcare/conditionsanddiseases/coronavirus/covid-19-infection-survey)
949 [diseases/coronavirus/covid-19-infection-survey](https://www.ons.gov.uk/peoplepopulationandcommunity/healthandsocialcare/conditionsanddiseases/coronavirus/covid-19-infection-survey)
(2021).

950 [32] Q. Bi, Y. Wu, S. Mei, C. Ye, X. Zou, Z. Zhang, X. Liu, L. Wei,
951 S. A. Truelove, T. Zhang, W. Gao, C. Cheng, X. Tang, X. Wu,
952 Y. Wu, B. Sun, S. Huang, Y. Sun, J. Zhang, T. Ma, J. Lessler,
953 T. Feng, Epidemiology and transmission of COVID-19 in 391 cases
954 and 1286 of their close contacts in Shenzhen, China: a retrospective
955 cohort study, *The Lancet Infectious Diseases* 20 (8) (2020) 911–919.
956 doi:10.1016/S1473-3099(20)30287-5.

957 [33] J. E. Lemieux, K. J. Siddle, B. M. Shaw, C. Loreth, S. F. Schaffner,
958 A. Gladden-Young, G. Adams, T. Fink, C. H. Tomkins-Tinch, L. A.
959 Krasilnikova, K. C. DeRuff, M. Rudy, M. R. Bauer, K. A. Lagerborg,
960 E. Normandin, S. B. Chapman, S. K. Reilly, M. N. Anahtar, A. E.
961 Lin, A. Carter, C. Myhrvold, M. E. Kemball, S. Chaluvadi, C. Cusick,
962 K. Flowers, A. Neumann, F. Cerrato, M. Farhat, D. Slater, J. B. Harris,

963 J. A. Branda, D. Hooper, J. M. Gaeta, T. P. Baggett, J. O'Connell,
964 A. Gnirke, T. D. Lieberman, A. Philippakis, M. Burns, C. M. Brown,
965 J. Luban, E. T. Ryan, S. E. Turbett, R. C. LaRocque, W. P. Hanage,
966 G. R. Gallagher, L. C. Madoff, S. Smole, V. M. Pierce, E. Rosenberg,
967 P. C. Sabeti, D. J. Park, B. L. MacInnis, Phylogenetic analysis of SARS-
968 CoV-2 in Boston highlights the impact of superspreading events, *Science*
969 371 (6529) (2021). doi:10.1126/science.abe3261.

970 [34] D. Miller, M. A. Martin, N. Harel, O. Tirosh, T. Kustin, M. Meir,
971 N. Sorek, S. Gefen-Halevi, S. Amit, O. Vorontsov, A. Shaag, D. Wolf,
972 A. Peretz, Y. Shemer-Avni, D. Roif-Kaminsky, N. M. Kopelman,
973 A. Huppert, K. Koelle, A. Stern, Full genome viral sequences inform
974 patterns of SARS-CoV-2 spread into and within Israel, *Nature Commu-*
975 *nications* 11 (1) (2020). doi:10.1038/s41467-020-19248-0.
976 URL <http://dx.doi.org/10.1038/s41467-020-19248-0>

977 [35] J. Riou, C. L. Althaus, Pattern of early human-to-human trans-
978 mission of Wuhan 2019 novel coronavirus (2019-nCoV), Decem-
979 ber 2019 to January 2020, *Eurosurveillance* 25 (4) (2020) 1–5.
980 doi:10.2807/1560-7917.ES.2020.25.4.2000058.
981 URL [http://dx.doi.org/10.2807/1560-7917.ES.2020.25.4.](http://dx.doi.org/10.2807/1560-7917.ES.2020.25.4.2000058)
982 2000058

983 [36] S. Chaudhuri, P. Kasibhatla, A. Mukherjee, W. Pan, G. Morrison,
984 S. Mishra, V. K. Murty, Analysis of overdispersion in airborne trans-
985 mission of Covid-19, (pre-print) (2021).
986 URL <https://doi.org/10.1101/2021.09.28.21263801>

- 987 [37] A. Goyal, D. B. Reeves, E. F. Cardozo-Ojeda, J. T. Schiffer, B. T.
988 Mayer, Viral load and contact heterogeneity predict sars-cov-2 transmis-
989 sion and super-spreading events, *eLife* 10 (2021) 1–63. doi:10.7554/
990 eLife.63537.
- 991 [38] J. Schijven, L. C. Vermeulen, A. Swart, A. Meijer, E. Duizer, A. M.
992 de Roda Husman, Quantitative microbial risk assessment for airborne
993 transmission of sars-cov-2 via breathing, speaking, singing, coughing,
994 and sneezing, *Environmental Health Perspectives* 129 (4) (2021) 1–10.
995 doi:10.1289/EHP7886.
- 996 [39] G. N. Sze To, C. Y. H. Chao, Review and comparison between the
997 wells–riley and dose-response approaches to risk assessment of infectious
998 respiratory diseases, *Indoor air* 20 (1) (2010) 2–16. doi:10.1111/j.
999 1600-0668.2009.00621.x.
- 1000 [40] L. M. Brosseau, K. Escandón, A. K. Ulrich, A. L. Rasmussen, C. J. Roy,
1001 G. J. Bix, S. V. Popescu, K. Moore, M. T. Osterholm, SARS-CoV-2
1002 Dose, Infection, and Disease Outcomes for COVID-19 – A Review, *Clinical Infectious Diseases* 54 (2021) 1–54. doi:10.1093/cid/ciab903.
1003 URL [https://academic.oup.com/cid/advance-article/doi/10.](https://academic.oup.com/cid/advance-article/doi/10.1093/cid/ciab903/6397523)
1004 [1093/cid/ciab903/6397523](https://academic.oup.com/cid/advance-article/doi/10.1093/cid/ciab903/6397523)
- 1006 [41] M. Cevik, K. Kuppalli, J. Kindrachuk, M. Peiris, *Virology*, transmission,
1007 and pathogenesis of SARS-CoV-2, *The BMJ* 371 (2020) 1–6. doi:10.
1008 1136/bmj.m3862.
- 1009 [42] M. Cevik, M. Tate, O. Lloyd, A. E. Maraolo, J. Schafers, A. Ho,

- 1010 SARS-CoV-2, SARS-CoV, and MERS-CoV viral load dynamics, du-
1011 ration of viral shedding, and infectiousness: a systematic review and
1012 meta-analysis, *The Lancet Microbe* 2 (1) (2021) e13–e22. doi:10.1016/
1013 S2666-5247(20)30172-5.
1014 URL [http://dx.doi.org/10.1016/S2666-5247\(20\)30172-5](http://dx.doi.org/10.1016/S2666-5247(20)30172-5)
- 1015 [43] Y. Pan, D. Zhang, P. Yang, L. L. Poon, Q. Wang, Viral load of SARS-
1016 CoV-2 in clinical samples, *The Lancet Infectious Diseases* 20 (4) (2020)
1017 411–412. doi:10.1016/S1473-3099(20)30113-4.
1018 URL [http://dx.doi.org/10.1016/S1473-3099\(20\)30113-4](http://dx.doi.org/10.1016/S1473-3099(20)30113-4)
- 1019 [44] S. Karimzadeh, R. Bhopal, H. Nguyen Tien, Review of infective
1020 dose, routes of transmission and outcome of COVID-19 caused
1021 by the SARS-COV-2: comparison with other respiratory viruses–
1022 CORRIGENDUM, *Epidemiology and Infection* 149 (2021) e116.
1023 doi:10.1017/S0950268821001084.
1024 URL [https://www.cambridge.org/core/product/identifier/
1025 S0950268821001084/type/journal_article](https://www.cambridge.org/core/product/identifier/S0950268821001084/type/journal_article)
- 1026 [45] R. Challen, E. Brooks-Pollock, J. M. Read, L. Dyson, K. Tsaneva-
1027 Atanasova, L. Danon, Risk of mortality in patients infected with SARS-
1028 CoV-2 variant of concern 202012/1: Matched cohort study, *The BMJ*
1029 372 (2021) 1–10. doi:10.1136/bmj.n579.
- 1030 [46] A. S. Walker, E. Pritchard, T. House, J. V. Robotham, P. J. Birrell,
1031 I. Bell, J. Bell, J. Newton, J. Farrar, I. Diamond, R. Studley, J. Hay,
1032 K.-D. Vihta, T. E. Peto, N. Stoesser, P. C. Matthews, D. W. Eyre,
1033 K. Pouwels, Ct threshold values, a proxy for viral load in community

- 1034 SARS-CoV-2 cases, demonstrate wide variation across populations and
1035 over time, *eLife* 10 (jul 2021). doi:10.7554/eLife.64683.
1036 URL <https://elifesciences.org/articles/64683>
- 1037 [47] B. Killingley, A. Mann, M. Kalinova, A. Boyers, N. Goonawardane,
1038 J. Zhou, K. Lindsell, J. Brown, R. Frise, E. Smith, C. Hopkins,
1039 N. Noulin, B. Londt, T. Wilkinson, S. Harden, Safety, tolerability and vi-
1040 ral kinetics during sars-cov-2 human challenge, *Nature Portfolio* (2022).
1041 doi:10.21203/rs.3.rs-1121993/v1.
1042 URL <https://doi.org/10.21203/rs.3.rs-1121993/v1>
- 1043 [48] G. Buonanno, L. Stabile, L. Morawska, Estimation of airborne viral
1044 emission: Quanta emission rate of SARS-CoV-2 for infection risk as-
1045 sessment, *Environment International* 141 (May) (2020) 105794. doi:
1046 10.1016/j.envint.2020.105794.
- 1047 [49] D. K. Milton, M. P. Fabian, B. J. Cowling, M. L. Grantham, J. J.
1048 McDevitt, Influenza Virus Aerosols in Human Exhaled Breath: Particle
1049 Size, Culturability, and Effect of Surgical Masks, *PLoS Pathogens* 9 (3)
1050 (2013). doi:10.1371/journal.ppat.1003205.
- 1051 [50] P. Fabian, J. J. McDevitt, W. H. DeHaan, R. O. Fung, B. J. Cowling,
1052 K. H. Chan, G. M. Leung, D. K. Milton, Influenza virus in human
1053 exhaled breath: An observational study, *PLoS ONE* 3 (7) (2008) 5–10.
1054 doi:10.1371/journal.pone.0002691.
- 1055 [51] K. K. Coleman, D. J. W. Tay, K. S. Tan, S. W. X. Ong, T. S. Than,
1056 M. H. Koh, Y. Q. Chin, H. Nasir, T. M. Mak, J. J. H. Chu, D. K. Milton,

- 1057 V. T. K. Chow, P. A. Tambyah, M. Chen, K. W. Tham, Viral Load of
1058 Severe Acute Respiratory Syndrome Coronavirus 2 (SARS-CoV-2) in
1059 Respiratory Aerosols Emitted by Patients With Coronavirus Disease
1060 2019 (COVID-19) While Breathing, Talking, and Singing, *Clinical
1061 Infectious Diseases 2 (Xx)* (2021) 1–7. doi:10.1093/cid/ciab691.
1062 URL [https://academic.oup.com/cid/advance-article/doi/10.
1063 1093/cid/ciab691/6343417](https://academic.oup.com/cid/advance-article/doi/10.1093/cid/ciab691/6343417)
- 1064 [52] F. K. Gregson, N. A. Watson, C. M. Orton, A. E. Haddrell, L. P. Mc-
1065 Carthy, T. J. Finnie, N. Gent, G. C. Donaldson, P. L. Shah, J. D.
1066 Calder, B. R. Bzdek, D. Costello, J. P. Reid, Comparing aerosol concen-
1067 trations and particle size distributions generated by singing, speaking
1068 and breathing, *Aerosol Science and Technology* 55 (6) (2021) 681–691.
1069 doi:10.1080/02786826.2021.1883544.
1070 URL <https://doi.org/10.1080/02786826.2021.1883544>
- 1071 [53] G. R. Johnson, L. Morawska, The mechanism of breath aerosol forma-
1072 tion, *Journal of Aerosol Medicine and Pulmonary Drug Delivery* 22 (3)
1073 (2009) 229–237. doi:10.1089/jamp.2008.0720.
- 1074 [54] G. R. Johnson, L. Morawska, Z. D. Ristovski, M. Hargreaves,
1075 K. Mengersen, C. Y. Chao, M. P. Wan, Y. Li, X. Xie, D. Kato-
1076 shevski, S. Corbett, Modality of human expired aerosol size distri-
1077 butions, *Journal of Aerosol Science* 42 (12) (2011) 839–851. doi:
1078 10.1016/j.jaerosci.2011.07.009.
- 1079 [55] L. Morawska, G. R. Johnson, Z. D. Ristovski, M. Hargreaves,
1080 K. Mengersen, S. Corbett, C. Y. Chao, Y. Li, D. Katoshevski, Size

1081 distribution and sites of origin of droplets expelled from the human res-
1082 piratory tract during expiratory activities, *Journal of Aerosol Science*
1083 40 (3) (2009) 256–269. doi:10.1016/j.jaerosci.2008.11.002.

1084 [56] O. O. Adenaiye, J. Lai, P. J. B. de Mesquita, F. Hong, S. Youssefi,
1085 J. German, S.-H. S. Tai, B. Albert, M. Schanz, S. Weston, J. Hang,
1086 C. Fung, H. K. Chung, K. K. Coleman, N. Sapoval, T. Treangen,
1087 I. M. Berry, K. Mullins, M. Frieman, T. Ma, D. K. Milton, *Infectious SARS-CoV-2 in Exhaled Aerosols and Efficacy of Masks During Early Mild Infection*, (pre-print) (2021). arXiv:2021.08.13.21261989, doi:<https://doi.org/10.1101/2021.08.13.21261989>, URL <https://doi.org/10.1101/2021.08.13.21261989>

1092 [57] V. M. Corman, I. Eckerle, T. Bleicker, A. Zaki, O. Landt, M. Eschbach-
1093 Bludau, S. van Boheemen, R. Gopal, M. Ballhause, T. M. Bestebroer,
1094 D. Muth, M. A. Müller, J. F. Drexler, M. Zambon, A. D. Osterhaus,
1095 R. M. Fouchier, C. Drosten, *Detection of a novel human coronavirus by real-time reverse-transcription polymerase chain reaction*, *Eurosurveillance* 17 (39) (2012) 1–6. doi:10.2807/ese.17.39.20285-en. URL <http://dx.doi.org/10.2807/ese.17.39.20285-en>